Improving the Calibration of Suomi NPP VIIRS Thermal Emissive Bands During Blackbody Warm-Up/Cool-Down

Wenhui Wang, Changyong Cao, Alexander Ignatov, Xingming Liang, Zhenglong Li, Likun Wang, Bin Zhang, Slawomir Blonski, and Jun Li

***Abstract*— The Suomi National Polar-orbiting Partnership Program Visible Infrared Imaging Radiometer Suite (VIIRS) thermal emissive bands (TEB) have been performing well during nominal operations since launch. However, small but persistent calibration anomalies are observed in all TEBs during the quarterly blackbody (BB) warm-up/cool-down (WUCD) events. As a result, the time series of daytime sea surface temperature (SST) (derived from bands M15–M16) show warm spikes on the order of 0.25 K. This paper suggests that VIIRS TEB WUCD biases are band dependent, with daily-averaged biases about −0.04 and 0.05 K for I4 and I5, and −0.05, −0.05, 0.11, 0.09, and 0.05 K for M12–M16, respectively. Two correction methods—Ltrace and WUCD-C—have been implemented and evaluated using colocated observations from the Cross-track Infrared Sounder (CrIS), radiative transfer simulations, and SST retrievals. Also an error in the National Oceanic and Atmospheric Administration operational processing was identified and fixed. Both correction methods effectively minimize WUCD-induced SST anomalies. The Ltrace method works well for I5, M12, and M14–M16, with residual biases about 0.01 K. The WUCD-C method, on the other hand, performs well to correct WUCD biases in all TEBs, with residual biases also about 0.01 K. However, it introduces warm biases relative to CrIS at cold scene temperatures, which requires further study. Applying nonequal BB thermistor weights improves calibration at BB temperature set points, but its impact on daily-averaged WUCD biases is small. The proposed methodologies may also be applied to the VIIRS onboard the follow-on Joint Polar Satellite System satellites.**

***Index Terms*— Blackbody (BB) warm-up/cool-down (WUCD), radiometric calibration bias, sea surface temperature (SST) anomaly, sensor data record (SDR), Suomi National Polar-orbiting Partnership (S-NPP), thermal emissive bands (TEB), Visible Infrared Imaging Radiometer Suite (VIIRS).**

Manuscript received December 24, 2017; revised July 5, 2018; accepted August 13, 2018. This work was supported by NOAA STAR through the Joint Polar Satellite System Program. *(Corresponding author: Wenhui Wang.)*

W. Wang, X. Liang, S. Blonski, and B. Zhang are with Earth Resources Technology, Inc., Laurel, MD 20707 USA (e-mail: wenhui.wang@noaa.gov).

C. Cao and A. Ignatov are with the NOAA/Center for Satellite Applications and Research, College Park, MD 20740 USA.

Z. Li and J. Li are with the Cooperative Institute for Meteorological Satellite Studies, University of Wisconsin–Madison, Madison, WI 53706 USA.

L. Wang and B. Zhang are with CICS/ESSIC, University of Maryland, College Park, MD 20740 USA.

Color versions of one or more of the figures in this paper are available online at http://ieeexplore.ieee.org.

Digital Object Identifier 10.1109/TGRS.2018.2870328

I. Introduction

THE Visible Infrared Imaging Radiometer Suite (VIIRS) onboard the Suomi National Polar-orbiting Partnership (S-NPP) satellite was successfully launched on October 28, 2011. The National Oceanic and Atmospheric Administration (NOAA) VIIRS sensor data records (SDRs), produced operationally by the interface data processing segment (IDPS), became available on January 20, 2012 and achieved validated maturity on March 19, 2014. VIIRS has seven thermal emissive bands (TEBs), including two imagery resolution bands (I4 and I5) and five moderate resolution bands (M12–M16), covering spectral range from 3.697 to 11.845 μm. S-NPP VIIRS TEB calibration has been performing well during nominal operations since launch. However, small but persistent calibration anomalies have been observed in all TEBs during the quarterly blackbody (BB) warm-up/cool-down (WUCD) events, which are performed to characterize on-orbit calibration offset and nonlinearity changes over time [1]–[3]. During such events, VIIRS daytime sea surface temperature (SST) product, which uses bands M15 and M16 as primary inputs, becomes anomalous with warm biases shown as spikes in the SST time series on the order of 0.25 K [4] as seen in the NOAA SST Quality Monitor system [5]. Accurate and stable satellite SST data are critical to numerical weather prediction, seasonal, and climate applications. The VIIRS TEB calibration anomalies during WUCD negatively impact the SST analysis according to the users, and therefore need to be addressed to better support these applications.

Cao *et al.* [1] analyzed the SST WUCD anomalies and attributed them primarily to a warm bias in M15 during the BB cooling phase of the WUCD, which is further amplified by the SST retrieval algorithm. The study suggests that the root cause of the WUCD calibration bias is the flawed theoretical assumption in the TEB calibration equations that the shape of the calibration curve remains unchanged on-orbit from that determined prelaunch. The assumption is not working well during the WUCD events when the temperature of BB is unstable. A localized correction method, with a diagnostic correction term (Ltrace), was introduced to reconcile the flawed assumption in the calibration algorithm and to significantly minimize the WUCD-induced calibration

bias in band M15. Three other approaches were also outlined, including: 1) performing more rigorous prelaunch analysis with identical WUCD condition as postlaunch on-orbit; 2) using calibration coefficients (C-coefficients) derived from on-orbit WUCD to improve the calibration (the WUCD-C method); and 3) adjusting the TEB radiometric model to make it work better under variable BB temperature conditions. Wang *et al.* [2] implemented and validated the Ltrace method. Preliminary results indicated that the method performs well for M15 and M16 and can minimize WUCD-induced SST anomalies. However, its performance in other TEBs, and the feasibility of other correction options, was not studied.

The goal of this paper is to analyze WUCD calibration biases in all S-NPP VIIRS TEBs and to investigate the alternative method and other potential improvements. The Ltrace and the WUCD-C methods were implemented, evaluated, and analyzed in-depth. This paper focuses on three unique aspects: 1) performance of the Ltrace method in all TEBs (recall that previous studies focused on M15 and M16 only); 2) feasibility of using on-orbit WUCD-derived C-coefficients; and 3) impacts of onboard BB temperature nonuniformity and an IDPS implementation error on TEB WUCD biases. The first satellite in the Joint Polar Satellite System (JPSS) series, NOAA-20 (previous named J1), was launched on November 18, 2017, with another VIIRS onboard, and three other JPSS satellites (J2–J4) will follow in the coming years. The methodologies developed in this paper may also be employed to improve the on-orbit calibration of VIIRS TEBs onboard all these JPSS satellites. This paper is organized as follows. VIIRS TEB calibration algorithm and S-NPP VIIRS TEB WUCD calibration biases are described in Section II. Section III presents the two WUCD bias correction methods. Section IV discusses validation results and impact on the SST product. Section V summarizes this paper.

II. VIIRS TEB Calibration Algorithm and Calibration Bias During WUCD

A. VIIRS TEB Calibration Algorithm

VIIRS has seven TEBs, including three midwave infrared (MWIR, I4 and M12 and M13) and four longwave infrared (LWIR, I5 and M14–M16) bands. I4 and I5 are imagery resolution bands (I-bands, 375-m spatial resolution at nadir); M12–M14 are moderate resolution bands (M-bands, 750-m spatial resolution at nadir). Table I summarizes spectral, spatial, and radiometric characteristics of these bands for S-NPP VIIRS [3], [6]. TEB on-orbit calibration depends on BB view, space view (SV), and some calibration parameters which have been characterized prelaunch. Details of VIIRS TEB calibration algorithm are described in previous publications [1], [7], [8]. The following equations show how the earth view (EV) radiances are calculated:

$$L_{\text{ev}} = \frac{F(c_0 + c_1 \times \text{dn} + c_2 \times \text{dn}^2) - (\text{RVS}_{\text{ev}} - 1) \times L_{\text{mirror}}}{\text{RVS}_{\text{ev}}} \tag{1}$$

$$L_{\text{mirror}} = \frac{(1 - \rho_{\text{RTA}}) L_{\text{RTA}} - L_{\text{HAM}}}{\rho_{\text{RTA}}} \tag{2}$$

TABLE I
Spectral, Spatial, and Radiometric Characteristics of VIIRS TEB Spectral Bands

	VIIRS TEBs	Center Wavelength (μm)	Spatial Resolution at nadir (m)	Ttyp (K, Spec.)	NEdT (K, On-Orbit)
MWIR	M12	3.697	750	270	0.12
	I4	3.753	375	270	0.4
	M13(high gain)	4.067	750	300	0.04
LWIR	M14	8.587	750	270	0.06
	M15	10.729	750	300	0.03
	I5	11.469	375	210	0.4
	M16	11.845	750	300	0.03

where L_{ev} is EV spectral radiance entering the instrument aperture, c_0, c_1, and c_2 are the C-coefficients derived from prelaunch test data, dn is the EV digital count with the SV digital count subtracted, RVS_{ev} is response versus scan at EV angle of incidence on the half-angle mirror (HAM), L_{mirror} is instrument background emission, ρ_{RTA} is the reflectivity of the rotating telescope assembly (RTA), and L_{RTA} is RTA-emitted radiance, and L_{HAM} is HAM-emitted radiance. F is on-orbit degradation factor (F-factor), which is computed based on the BB and SV observations for each scan

$$F = L_{\text{model}} / L_{\text{prelaunch}} \tag{3}$$

$$L_{\text{model}} = \text{RVS}_{\text{bb}}(\varepsilon_{\text{bb}} L_{\text{bb}} + (1 - \varepsilon_{\text{bb}}) \times L_{\text{env}}) + (\text{RVS}_{\text{bb}} - 1) \times L_{\text{mirror}} \tag{4}$$

$$L_{\text{prelaunch}} = c_0 + c_1 \times \text{dn}_{\text{bb}} + c_2 \times \text{dn}_{\text{bb}}^2 \tag{5}$$

where RVS_{bb} is response versus scan at BB angle of incidence on the HAM, ε_{bb} is BB emissivity, L_{bb} is BB spectral radiance according to Planck's function, $(1 - \varepsilon_{\text{bb}}) \times L_{\text{env}}$ is BB shield, cavity, and telescope originated radiance reflected off the BB; and dn_{bb} is the BB digital count with the SV digital count subtracted. Note M13 is a dual-gain band. Its low-gain mode, intended for fire detection, has a temperature range (343–634 K) that is significantly higher than the maximum BB temperature (315 K). Therefore, only M13 high-gain state is considered in this paper.

Following the heritage of the Moderate Resolution Imaging Spectroradiometer (MODIS) [9], quarterly WUCDs are performed to characterize VIIRS TEB on-orbit calibration offset (c_0) and nonlinearity (c_2) changes over time. A typical WUCD event usually lasts three days (except for the first two extended WUCD events in the beginning of the mission, February 6, 2012–February 10, 2012 and May 22, 2012–February 25, 2012). During the warm-up phase, BB temperature is first raised stepwise from its nominal setting of 292.5 K to 297.5, 302.5, 307.5, 312.5, and 315 K. After that, the heater is turned off, and the cool-down (CD) phase begins, during which the BB temperature drops from 315 to about 267 K.

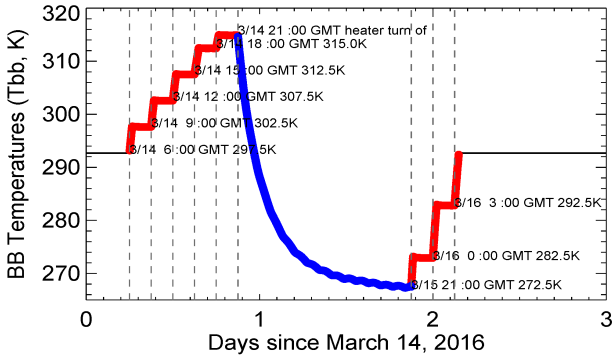

Fig. 1. BB temperature sequences during the March 14, 2016–March 16, 2016 WUCD event. The warm-up phase is shown in red; the CD phase is shown in blue.

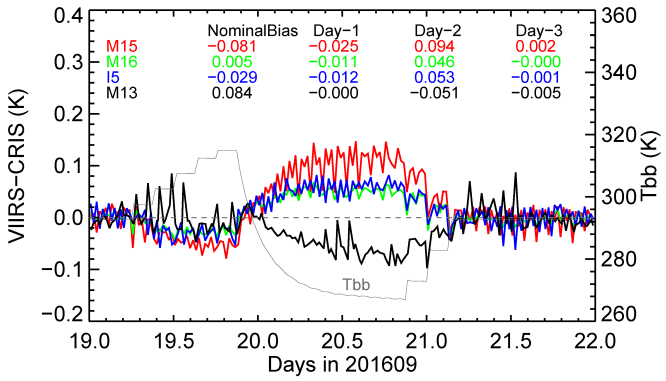

Fig. 2. VIIRS–CrIS BT difference time series during the September 19, 2016–September 21, 2016 WUCD event.

Then, the BB temperature is brought back to its nominal level in three steps, by first raising it to 272.5 K, then to 282.5 K, and finally to 292.5 K. In this paper, this latter phase is also referred to as the warm-up phase. Fig. 1 illustrates a typical time series of the BB temperature during a 3-day WUCD event.

B. VIIRS TEB WUCD Calibration Biases in the NOAA Operational Processing

The NOAA operational VIIRS TEB calibration has been performing generally well during nominal operations since launch. One major issue, initially noticed by the SST Team and later investigated in individual bands by the VIIRS SDR Teams, is the small but persistent biases in all TEBs during the WUCD events, which are amplified in SST retrievals. Fig. 2 shows time series of VIIRS minus Cross-track Infrared Sounder (CrIS is also onboard S-NPP) brightness temperature (BT) differences in bands I5, M13, M15, and M16 during the September 19, 2016–September 21, 2016 WUCD event. Details about the VIIRS and CrIS colocation and intercomparison method are given in Section IV-A. VIIRS–CrIS nominal biases (calculated when the BB temperature is nominal, i.e., before and after WUCDs) were subtracted from the time series. As a result, the biases are close to zero during the nominal operations. Daily-averaged VIIRS WUCD biases for Day 1 (dominated by the warm-up phase), Day 2 (dominated by the CD phase), and Day 3 (very close to nominal operations) are calculated as the difference between VIIRS and CrIS biases at all BB temperatures. While CrIS calibration is unchanged, VIIRS–CrIS time series reveal that the VIIRS TEB calibration becomes unstable during the WUCD event. Bias patterns in LWIR bands (M15, M16, and I5) are similar, featuring small negative biases on Day 1 and larger positive biases on Day 2. The MWIR band (M13), however, exhibits a different pattern, with a negative bias on Day 2. The Day-2 biases, which dominate WUCD biases, are about +0.05, −0.05, +0.09, and +0.05 K in I5, M13, M15, and M16, respectively. WUCD biases during Day 3 are negligible. Very similar bias patterns are also observed during other WUCD events.

Chang and Xiong [10] assessed the impacts of uncertainties in BB emissivity, BB uniformity, cavity emission, RTA emission, and nonlinear calibration coefficient on MODIS TEB calibration. VIIRS TEB on-orbit calibration is similar to MODIS. We also analyzed the sensitivity of various calibration terms in the VIIRS calibration equations to the WUCD bias. However, our results indicate that it is very challenging to pin point the exact factor(s) responsible for the WUCD calibration biases, among tens of terms. In Sections II-D–II-E, we focus on three factors, including BB nonuniformity, error in the IDPS C-coefficients implementation, and F-factor anomaly during WUCD. Other factors (such as errors in ε_{bb}, RVS_{bb}, RTA, and/or HAM emission, and relative spectral response function) may also contribute to the TEB calibration biases during WUCD, but they are out of the scope of this paper. Moreover, this paper focuses on WUCD biases, and VIIRS calibration biases during the nominal operations, such as scene temperature-dependent biases (see Section IV-A), are also out of the scope of this paper.

C. VIIRS Blackbody Nonuniformity

Accurate BB temperature measurements are one prerequisite for reliable on-orbit VIIRS TEB calibration. The S-NPP VIIRS BB has been carefully characterized prelaunch using the National Institute of Standard and Technology external traceable BB calibration source. The emissivity of the BB is high ($\varepsilon_{bb} > 0.996$). VIIRS uses six thermistors embedded in the BB to provide accurate temperature measurements from its different parts at each scan. Thermistors 1 and 4 (T_1 and T_4) are closer to the EV port, while thermistors 3 and 6 (T_3 and T_6) are closer to the solar diffuser port. During normal operations, BB temperature is set to the nominal value of 292.5 K.

Fig. 3 shows time series of BB uniformity (defined as standard deviation of six thermistor temperatures) and individual BB thermistor temperature anomalies (individual thermistor temperature readings minus average temperature of the six thermistors) during nominal operations (before March 14, 2016 6:00 GMT and after March 16, 2016 3:00 GMT) and during WUCD (March 14, 6:00 GMT–March 16 3:00 GMT, 2016). To put these results in proper context, the spacecraft solar zenith angle (SC_SZA) is also plotted in the background in Fig. 3(a). S-NPP VIIRS BB temperature is highly uniform during the nominal operations, with uniformity on the order of 20 mK. BB is slightly less uniform during daytime (SC_SZA < 90°), while BB uniformity

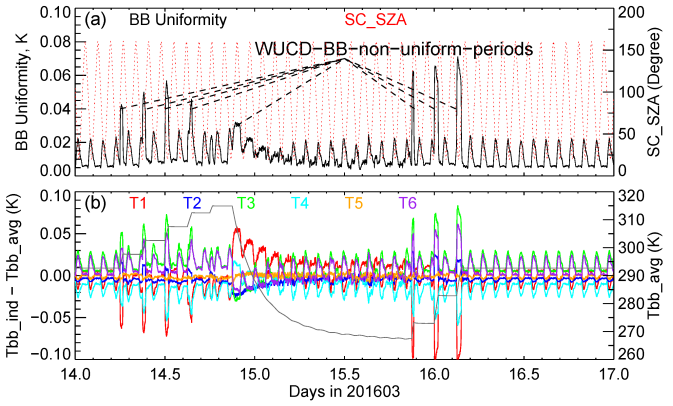

Fig. 3. Time series of (a) BB uniformity (defined as standard deviation of temperatures of six thermistors) and (b) anomalies of individual BB thermistor temperature (individual thermistor temperature readings minus average temperature of the six thermistors). Nominal operations took place before March 14, 2016 6:00 GMT and after March 16, 2016 3:00 GMT. WUCD event was conducted from March 14, 6:00 GMT to March 16 3:00 GMT, 2016.

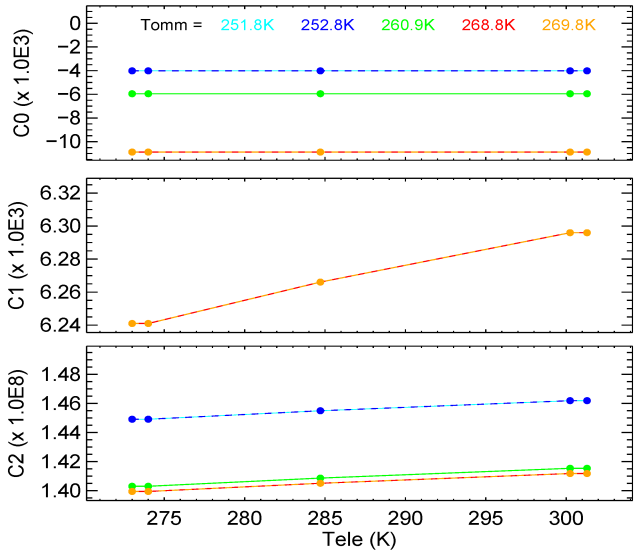

Fig. 4. Examples of prelaunch C-coefficients for M15 (electronic side-B, HAM-A, detector 1).

is better than 10 mK during nighttime (SC_SZA > 90°). T_1 and T_4 readings are a little lower, and T_3 and T_6 readings are a little higher than those of T_2 and T_5. During a WUCD, the BB uniformity is consistent with that during the nominal operations, most of the time. However, larger nonuniformities are observed at BB temperature set points (see Fig. 1) and during the initial 2 and 3 orbits of the CD phase (in the rest of this paper, these short periods are referred as WUCD-BB-nonuniform periods).

Up until this analysis, equal BB thermistor weights have been used in the NOAA VIIRS operational processing (OPR). During the nominal operations, and most of the time duringto the WUCDs, the impact of BB nonuniformity on TEB calibration is on the order of 0.01 K. However, during the BB-nonuniform periods (which occur in ∼7.5% of the 21 h of WUCD events), the error can exceed 0.05 K. Our results indicate that BB nonuniformity has only a minor contribution TEB WUCD calibration bias, but it is not the dominant factor.

To improve TEB calibration during the WUCD-BB-nonuniform periods, a set of nonequal BB thermistor weights (NW, T_1: 2.543e^{-5}, T_2: 8.551e^{-2}, T_3: 0.6780, T_4: 2.456e^{-4}, T_5: 2.823e^{-3}, T_6: 0.2334) were developed in this paper and used in conjunction with the WUCD bias correction methods presented in Section III. Current IDPS code only allows one set of weights for all bands. Nonequal weights were first estimated for individual bands, detectors, and HAM sides by minimizing residual errors of WUCD-derived C-coefficients (see Section III-B). The basis of this approach is that effective nonequal weights should reduce data scattering and minimize on-orbit WUCD C-coefficients fitting errors. Then, one set of nonequal weights was calculated by averaging all weights. Our results show that in all cases, T_3 and T_6 (which are closer to the solar diffuser port) contribute consistently heavier, among the six BB thermistors. The impacts of the nonequal BB thermistor weights will be further discussed in Sections III and IV.

D. Error in Operational Implementation of C-Coefficient Instrument Temperature Dependence

VIIRS TEB detector and electronic responses vary with instrument temperature [8]. During prelaunch characterization, three sets of C-coefficients were derived for each detector, HAM side, and band using thermal vacuum data, corresponding to the cold, nominal, and hot instrument temperature plateaus. In the NOAA OPR, the three sets of C-coefficients were extrapolated to a [5 optomechanical temperatures (T_{omm}) × 5 electronics temperatures (T_{ele})] grid, to account for on-orbit instrument temperature variations over time. Fig. 4 shows an example of prelaunch C-coefficients for M15 (electronic side-B, HAM-A, detector 1).

A discrepancy between the JPSS Data Format Control Book (CDFCB) [11] and the IDPS VIIRS SDR code was identified in this paper. The CDFCB states that T_{ele} is the faster moving dimension and T_{omm} is the slower moving dimension. While the VIIRS C-coefficients lookup table (VIIRS-SDR-DELTA-C-LUT) follows the CDFCB definition, the two dimensions are switched in the IDPS software. Variations of T_{omm} and T_{ele} are different over time, especially during the WUCDs. This implementation error results in errors in the actual C-coefficients used in the operational calibration of both VIIRS reflective solar bands (RSBs) and TEBs. This discrepancy can be resolved by either a code change or a C-coefficient LUT and documentation update. The latter option, which is significantly faster to implement operationally, was adopted and implemented in IDPS on April 5, 2018 for S-NPP. Here, we focus on its impacts on the TEB calibration.

Fig. 5 shows time series of c_0, c_1, c_2, F-factor (F), and $F \cdot c_1$ during the March 2016 WUCD event, before and after the fix of this error, for two VIIRS bands—M15 and M16 (HAM-A, detector 1). The patterns are similar for other LWIR bands, detectors, and HAM-B. The error has noticeable impact on all terms during both nominal and WUCD operations.

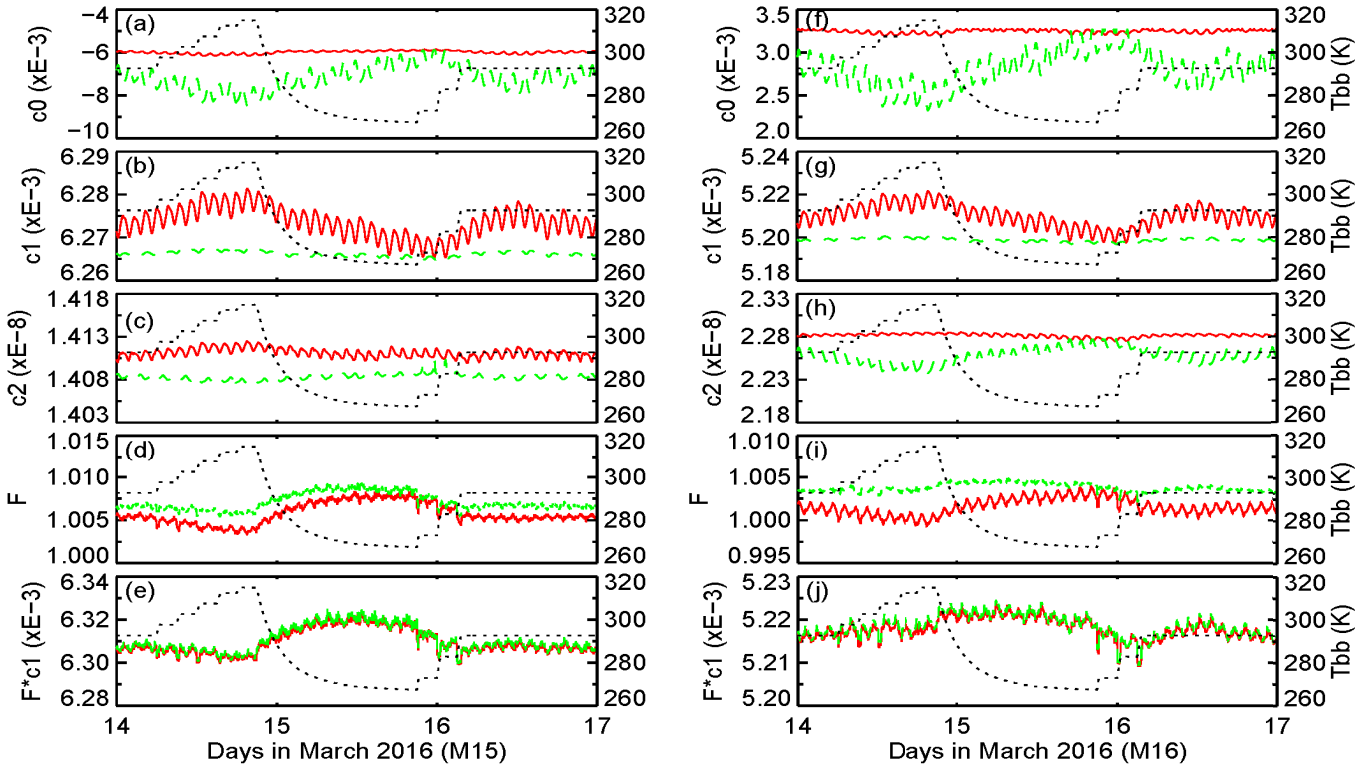

Fig. 5. Time series of granule averaged c_0, c_1, c_2, F-factor (F), and $F \cdot c_1$ for (a)–(e) M15 and (f)–(j) M16 (HAM-A, detector 1) during the March 2016 WUCD event, (red curves) before and (green curves) after the correction of the IDPS C-coefficient implementation error. BB temperature is plotted in the background in gray, for reference.

After correction, the orbital variations become smaller in c_1, c_2, and F-factor and larger in c_0. For the MWIR bands, the impact on the c_0 and c_2 is similar to those for the LWIR bands, while the impacts on c_1 and F-factor are significantly smaller.

Due to the high linearity of detector responses and BB-based on-orbit calibration, the impact of the error on the term $F \cdot c_1$, which dominates the SDR radiometric calibration, is rather small ($\sim$0.01%) because its effects on the c_1 and F-factor are in the opposite directions, and therefore, mostly cancel out each other. Therefore, it does not cause dramatic calibration errors in the current operational SDR products, and only minimally affects the cold and hot scenes. During the nominal operations, in M15 and M16, the implementation error causes calibration biases up to about -0.05 and -0.02 K at 200-K scene temperature, respectively; at 290-K scene temperature, the impact is about 0 and $+0.02$ K in M15 and M16, respectively. At 315-K BB temperature, the impact on both bands doubles, especially at cold scene temperatures.

However, this implementation error has large impact on a bias correction method that empirically adjusts the F-factors during WUCDs based on F-factor during nominal operations, such as the Ltrace method proposed by Cao *et al.* [1]. The Ltrace attempts to correct WUCD bias by flattening the F-factor, using a correction term estimated from the F-factors during the nominal operations and WUCD, which are both affected but with different magnitudes. In this paper, the Ltrace correction term will be estimated after the correction of this error. This is further discussed in Section III-A. The error will be referred as the IDPS C-coefficients implementation error in the rest of this paper.

E. F-Factor Anomalies During WUCDs

Sections II-C and II-D show that the nonuniformity of the BB and the IDPS C-coefficients implementation error both affect the TEB calibration, especially during the WUCDs. However, their impacts are relatively small and therefore cannot explain the observed TEB WUCD biases.

Consistent with Cao *et al.* [1], our analyses suggest that during the WUCDs, the TEB calibration bias is dominated by changes in the calibration curve (F-factor anomalies). Fig. 6 shows time series of the band-averaged F-factors in all TEBs during the September 2016 WUCD event. To put these results in perspective, sensitivities of TEB scene temperatures to a hypothetical 0.1% anomaly in F-factor (theoretically calculated based on Planck's function), are given in Fig. 7. F-factors during other WUCD events show similar anomaly patterns. Day-2 (September 20, 2016) average F-factor anomaly (in percent), and the corresponding WUCD biases estimated at 290-K scene temperature (which is close to global mean temperature of the EV), are also shown.

It is observed that during the nominal operations, the F-factors are very stable, except for small orbital variations. During the WUCDs, the variations in the F-factors become much larger, and occur largely in sync with the changes in the BB temperature. Moreover, they track closely the

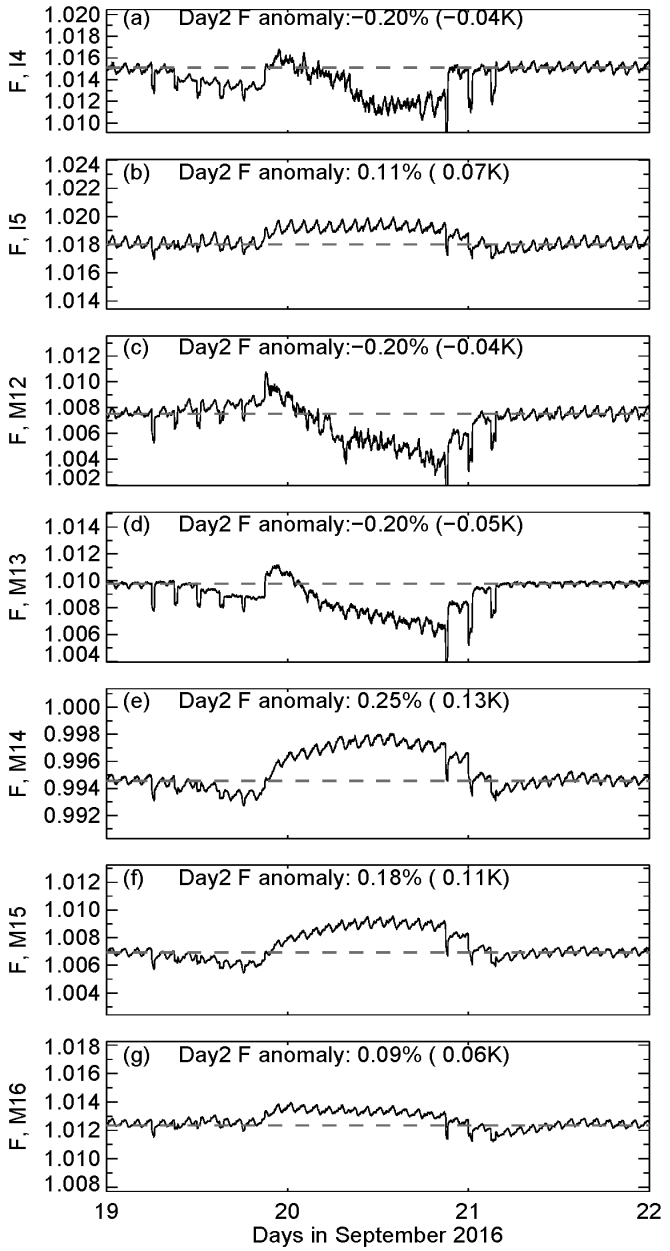

Fig. 6. Time series of band-averaged F-factors for (a) and (b) I4 and I5 and (c)–(g) M12–M16 during the September 2016 WUCD.

WUCD biases observed in the VIIRS–CrIS biases plotted in Fig. 2. For more quantitative comparisons, the Day-2 F-factor anomalies in Fig. 6 have been converted to BT biases using the sensitivity chart in Fig. 7 at 290-K scene temperature. Those are −0.04 and +0.07 K in I4 and I5, and −0.04, −0.05, +0.13, +0.11, and +0.06 K in M12–M16, respectively. Note that these estimated biases are due to the F-factor anomaly only. WUCD biases may also be affected by other factors, including (but not limited to) the BB nonuniformity and the IDPS C-coefficients implementation error. Nevertheless, the WUCD biases estimated from the F-factor anomalies generally agree with the WUCD biases derived using colocated CrIS observations in bands I5, M13, M15, and M16 (see Fig. 2), which are direct estimations and therefore are more reliable. Note that M12–M16 WUCD biases are also independently estimated using radiative transfer simulations in Section IV-B, but no validation data are available for band I4 so far to independently verify its WUCD bias (−0.04 K) estimated from the F-factor WUCD anomaly.

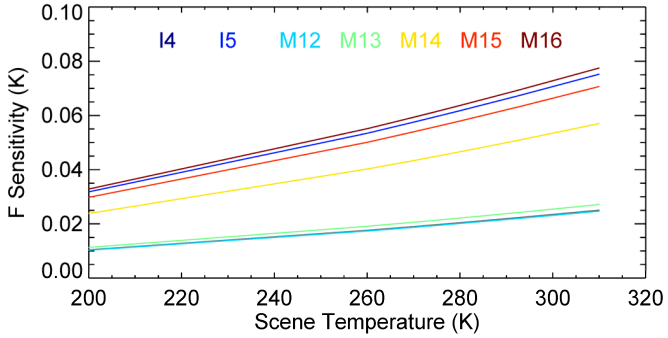

Fig. 7. Sensitivity of scene temperatures to a hypothetical 0.1% anomaly in F-factor (theoretically calculated based on Planck's function. Curves for I4 and M12 overlap each other).

III. Methods for TEB WUCD Calibration Bias Correction

Our analyses in Section II largely support the earlier observation by Cao *et al.* [1] that the VIIRS WUCD biases are primarily caused by the anomalies in the corresponding F-factors. This paper further analyses the two correction methods proposed by Cao *et al.* [1], the Ltrace and the WUCD-C, based on reconciling the F-factor changes, discusses the impact of the BB nonuniformity, and fixes the IDPS C-coefficient implementation error.

A. Ltrace Method

The use of on-orbit scan by scan F-factor is a unique characteristic of VIIRS. The Ltrace method introduces an additive correction term, Ltrace, to the F-factor equation, to minimize the calibration biases during the WUCDs by mitigating the changes in the shape of the calibration curve. Details of this method are found in Cao *et al.* [1]. The following equations show the modified F-factor equation and the definition of the Ltrace term:

$$F = (L_{\text{model}} + L_{\text{trace}})/L_{\text{prelaunch}} \tag{6}$$

$$L_{\text{trace}} = F_{\text{norm}} \times L_{\text{prelauch}} - L_{\text{model}}. \tag{7}$$

The Ltrace term is derived numerically using dn_{bb}, averaged F-factor over multiple orbits during nominal operations (F_{norm}, at $T_{\text{bb}} = 292.5$ K), prelaunch C-coefficients, and the L_{model} term [defined by (4)] during the WUCD. This method assumes that the shape of the calibration curve during the WUCD and derived prelaunch can be matched by flattening the F-factor. The Ltrace method is designed to be a localized correction, which is only applied during the WUCD. The idea behind this method is that although one cannot fully validate (or otherwise) the calibration-shaped curve assumption, the current algorithm works well enough in producing a consistent SST product outside the WUCD events. Therefore, one only needs to perform a correction during the WUCD period [1].

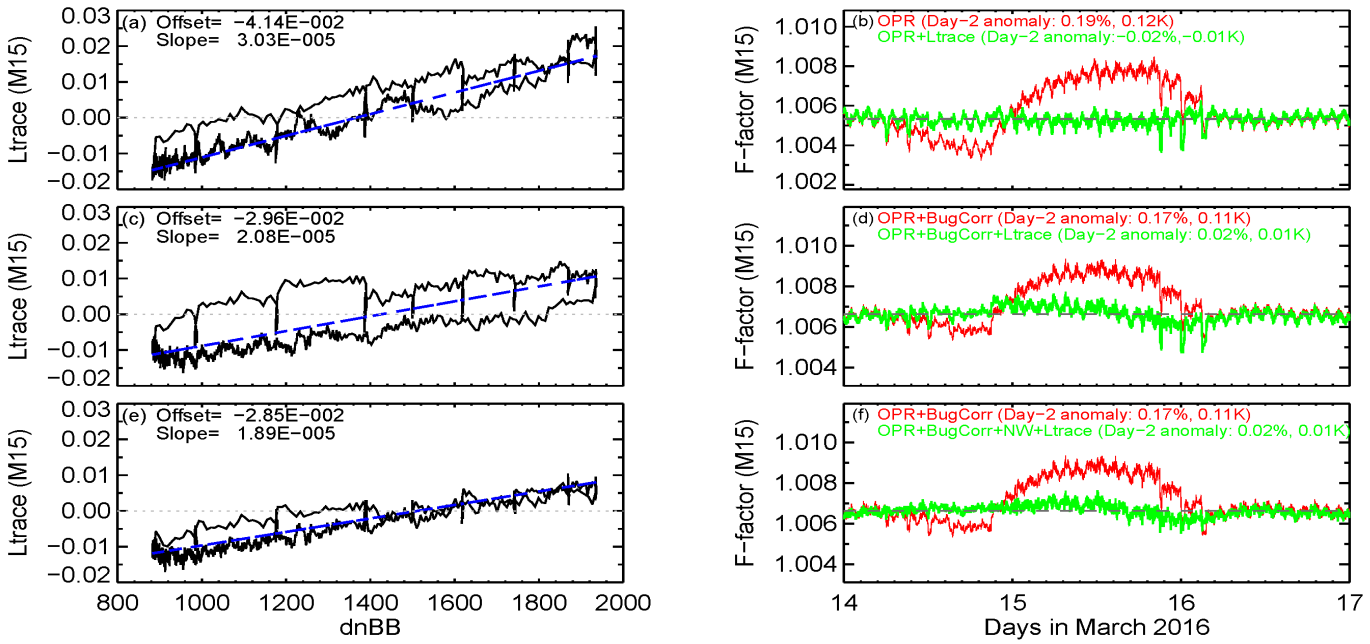

Fig. 8. (a), (c), and (e) Example of the Ltrace coefficients, offset, and slope, for M15 (detector 1, HAM-A) and (b), (d), and (f) time series of band-averaged (in M15) F-factor during the March 2016 WUCD (red curves) before and (green curves) after the Ltrace correction. (a) and (b) Before the correction of the IDPS C-coefficients implementation error and using equal BB thermistor weights. (c) and (d) After the correction of the C-coefficients implementation error (BugCorr). (e) and (f) After additionally applying nonequal BB thermistor weights (NW). The black lines in (a), (c), and (e) show Ltrace term [see (7)] as a function of $\mathrm{dn_{bb}}$; the fit line defined by the Ltrace coefficients is shown in blue dashed lines.

Wang *et al.* [2] presented preliminary results for the operational implementation and validation of the Ltrace method in M15 and M16. This paper further investigates this method for all TEBs. Band, detector, and HAM-side dependent linear correction coefficients (Ltrace offset and slope) were fit using all data during the WUCD event. Fig. 8 shows the Ltrace correction coefficients for M15 (detector 1, HAM-A), along with time series of band-averaged F-factors during the March 2016 WUCD. The three rows correspond to: 1) current NOAA operational data; 2) after the correction of the IDPS C-coefficients implementation error; and 3) after additionally applying nonequal BB thermistor weights (given in Section II-C). Corresponding time series of F-factors before and after the Ltrace correction are also shown. Note that the data during the WUCD-nonuniform periods were not used to derive the Ltrace coefficients, to minimize (for the first two cases) the impact by the low-quality data due to nonuniform BB thermistor readings, on the correction coefficients.

Daily-averaged F-factor anomalies on Day 2, as well as their corresponding biases estimated at 290-K scene temperature, are shown in Fig. 8 (right). As discussed in Section II-D, the C-coefficients implementation error has large impact on the Ltrace correction coefficients. After its correction, the Ltrace offsets and slopes both become about 30% smaller [see Fig. 8(a) and (c)]. The impact of the error on the Ltrace method is further discussed in Section IV-A using validation results. It is also observed that the Ltrace correction reduces the F-factor anomaly from 0.18% to 0.02% [corresponding to a WUCD bias reduction from 0.11 to 0.01 K at 290-K scene temperature, see Fig. 8(d)]. Applying nonequal BB thermistor weights produce more stable calibration at pixel/scan/granule levels by further reducing the orbital variations in the F-factor, and minimize the anomalies during the WUCD-BB-nonuniform periods [see Figs. 3 and 8(d) and (f)]. However, its impacts on the daily-averaged WUCD biases are small, with Day-2 F-factor anomaly remaining the same before and after applying the nonequal BB thermistor weights [see Fig. 8(d) and (f)]. Similar patterns were observed for other M15 detectors, HAM-B, and during other WUCD events.

Fig. 9 shows band-averaged F-factors before and after the Ltrace correction for I4, I5, M12–M14, and M16 during the March 2016 WUCD event. The IDPS C-coefficients implementation error was corrected and nonequal BB thermistor weights were applied in all bands. Day-2 averaged F-factor anomalies (in percent) and the corresponding WUCD biases (estimated at 290-K scene temperature) are also shown. The Ltrace method works well for the LWIR bands, with Day-2 F-factor anomalies reduced from 0.11%, 0.26%, and 0.09% to 0.04%, 0.03%, and 0.04%, for I5, M14, and M16, respectively. The method also flattens the F-factor in M12, with Day-2 anomaly reduced from −0.19% to 0.03%. The nonequal BB thermistor weights work effectively for all TEBs, with the dips in the time series of the F-factors cased by BB nonuniformity signifiantly reduced. Our validation results suggest that the residual F-Factor anomalies after the Ltrace correction are small enough to minimize WUCD biases in I5, M12, and M14–M16 (see Section IV).

One set of Ltrace coefficients (offsets and slopes) derived using the March 2016 WUCD data works well for all LWIR bands and M12 during all WUCD events since launch. Fig. 10 shows time series of band-averaged normalized F-factors before and after the Ltrace correction for

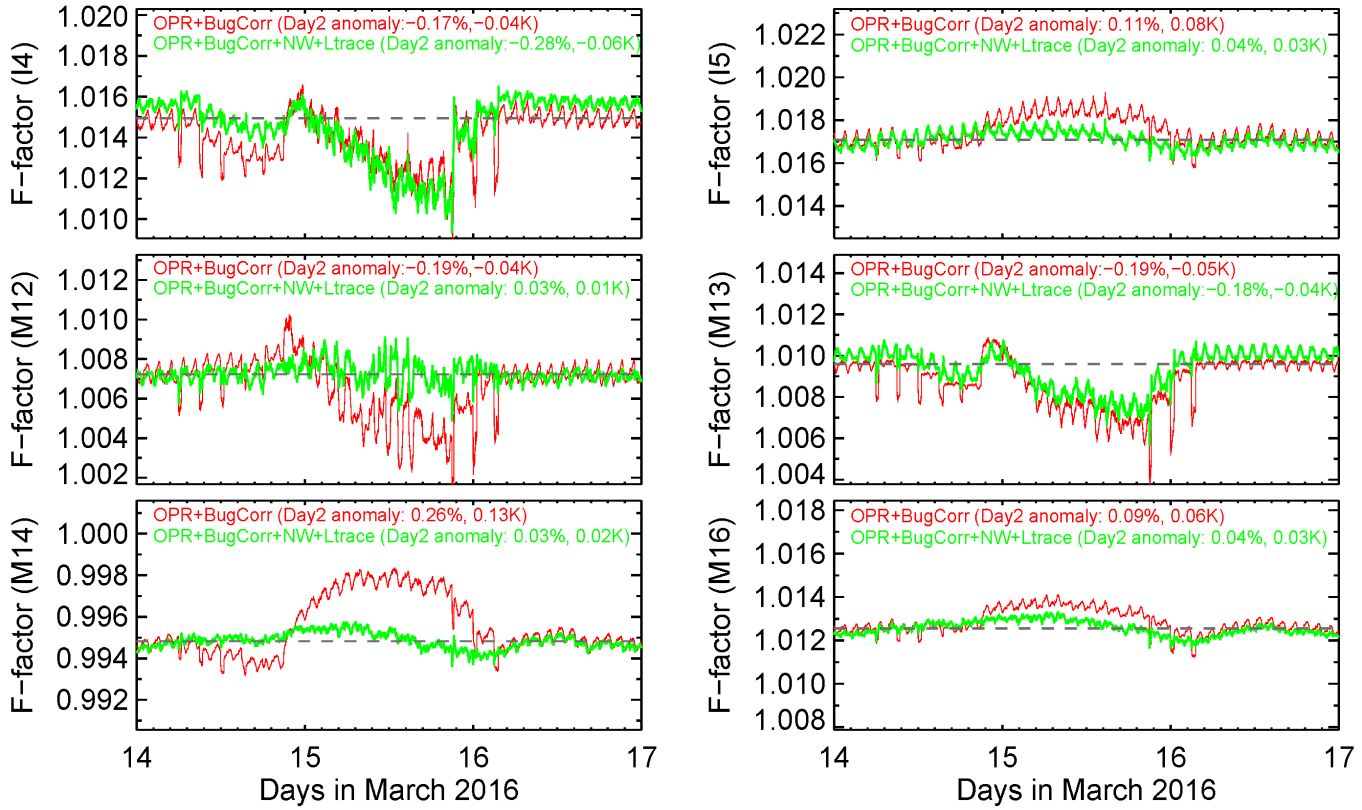

Fig. 9. Time series of band-averaged F-factor (red curves) before and (green curves) after the Ltrace correction for I4 and I5, M12–M14, and M16 for the March 2016 WUCD. The IDPS C-coefficients implementation error (BugCorr) is corrected and nonequal BB thermistor weights (NW) are applied in all bands.

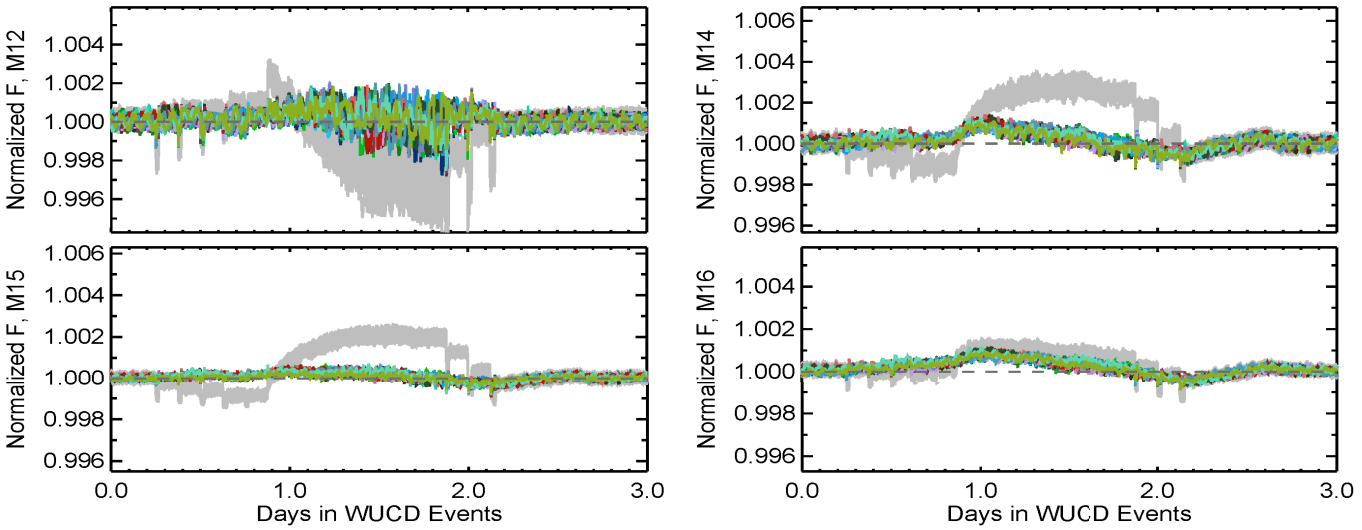

Fig. 10. Time series of nomalized band-averaged F-factor (gray) before and after the Ltrace correction in the three VIIRS TEBs currently used for SST retrievals and soon-to be added M14. Overlaid are 18 WUCD events from September 2012 to December, 2016. F-factors for individual WUCD events are plotted using different colors.

the 18 3-Day WUCD events from September 2012 to December 2016, in all VIIRS bands currently used for SST retrievals, including M12, M15, and M16 and soon to be added M14. Normalized F-factors before the correction are plotted in the background (gray). Patterns of residual F-factor anomalies are very close to each other for all WUCD events. Similar residual F-factor anomalies were also observed during the February and May 2012 WUCD events (which are not shown, due to their longer and different WUCD schedules).

In the I4 and M13, the Ltrace terms are correlated with dn_{bb} much more loosely. As a result, linear Ltrace coefficients do not work well in these two MWIR bands. We also considered forcing TEB F-factors to constant values estimated during nominal operations right before a WUCD event.

This potential simple solution makes F-factors absolutely flat during WUCD. However, nominal F-factors change over time due to instrument response degradation and therefore require periodical updates, especially for I5 that shows more pronounced degradation since launch based on the monitoring results in the NOAA STAR's Integrated Calibration Validation System [12]. The Ltrace correction coefficients fit using data during the CD phase, as well as using higher order polynomials, were also investigated. But the results for I4 and M13 were not significantly improved. Fitting the Ltrace coefficients using more sophisticated models may improve WUCD bias correction results. While the Ltrace method is empirical, an improved version (Ltrace-2) that reconciles the calibration curve changes analytically was developed [13]. Here, we only assess the original Ltrace method. More work is needed to implement and evaluate these additional options, and those will be studied in the future.

B. WUCD-C Method

The WUCD-C method is another option proposed by Cao *et al.* [1]. Similar method has been used to calibrate MODIS TEBs [9], [10]. On-orbit BB WUCD provides a source of calibration radiance over the range from ~267 to 315 K [3], independent of prelaunch calibration source. HAM-side and detector-specific second-order polynomial C-coefficients can be fit using WUCD data with the following equation:

$$\begin{aligned} c_0 + c_1 \times \mathrm{dn}_{\mathrm{bb}} + c_2 \times \mathrm{dn}_{\mathrm{bb}}^2 \\ = \mathrm{RVS}_{\mathrm{bb}}[\varepsilon_{\mathrm{bb}} L_{\mathrm{bb}} + (1-\varepsilon_{\mathrm{bb}}) \times L_{\mathrm{env}}] \\ + (\mathrm{RVS}_{\mathrm{bb}} - \mathrm{RVS}_{\mathrm{sv}}) \times L_{\mathrm{mirror}}. \end{aligned} \tag{8}$$

On-orbit instrument environment may be different from prelaunch. The WUCD-C method assumes that the C-coefficients derived from on-orbit WUCD data may better represent on-orbit conditions. Similar to the Ltrace method, the WUCD-C method also assumes that the F-factor should be flat, consistent with Cao *et al.* [1] on the point that the instrument response should remain the same when its BB temperature changes.

It is worth noting that the on-orbit WUCD-derived C-coefficients may be subject to two potential limitations. First, T_{omm} and T_{ele} are well controlled in the prelaunch environment and separate C-coefficients, at cold, nominal, and hot plateaus, can be derived to account for calibration curve changes at different instrument temperatures. On-orbit, however, data at a wide range of T_{omm} and T_{ele} have to be combined, to derive one set of WUCD C-coefficients, and no instrument temperature dependence can be accounted for (equivalent to an implicit assumption that the sensitivity of the C-coefficients to instrument temperature is negligible). In other words, the WUCD-C method attempts to flatten not only the F-factor, but also the $F \cdot c_1$ term. As a result, the WUCD-C method is not affected by the IDPS C-coefficients implementation error discussed in Section II-D, due to an implicit lack of instrument temperature dependence in WUCD-derived C-coefficients. Second, on-orbit WUCD data cover only a limited range of radiances (BB temperature varying from ~267 to 315 K), compared to prelaunch test data (where it was varied from 190 to 345 K). The performance of the WUCD-derived C-coefficients may be thus limited for the scene temperatures outside of the WUCD range.

Different subsets of WUCD data could be selected to derive on-orbit WUCD C-coefficients. Since the F-factor anomalies and WUCD biases peak at BB temperature close to 267 K during the CD phase (see Figs. 2 and 9), the C-coefficients derived from a subset without the CD data cannot effectively flatten the F-factors. In this paper, we only analyze C-coefficients estimated using the following three subsets of data that all include the data collected during the CD phase.

1) CD only would optimize calibration for scene temperatures close to 267 K because more data are available near this temperature. (WUCD biases are the most prominent at this BB temperature).
2) All data during a 3-/4-/5-day WUCD cycle (WUCD + All) optimizing calibration at scene temperatures close to 292.5 K due to the fact that more than one-third of data used are at nominal BB temperatures.
3) All data during the actual WUCD plus 100 granules during the nominal operations before a WUCD event (WUCD + 100), compromising calibration at all temperatures, with slightly higher priority given to scene temperature close to 267 K.

Fig. 11 shows M15 (detector 1, HAM-A) C-coefficients fit using the three subsets of data, as well as time series of band-averaged $F \cdot c_1$, generated using the prelaunch and the on-orbit WUCD derived C-coefficients. Unstable data during the dark current restore changes were excluded. Nonequal BB thermistor weights were used in all cases. Residual errors (predicted—modeled radiance) from the second-order polynomial fits are generally within 0.005 W/(m^2 · sr · μm), approximately about 0.15 and 0.03 K at 200- and 300-K scene temperatures, respectively. It can be observed that the WUCD C-coefficients derived using the three subsets can generally flatten the $F \cdot c_1$ time series. In addition, the WUCD C-coefficients also reduce orbital $F \cdot c_1$ variations during nominal operations.

Fig. 12 summarizes, for LWIR (I5, M14–M16), band-averaged C-coefficients derived using the three subsets for all WUCD events from 2012 to 2016. Band-averaged prelaunch C-coefficients are also plotted for comparison purpose. LWIR bands generally show little degradation from 2012 to 2016, except for band I5, which shows a 0.3%–0.4% per year degradation in linear response, generally consistent with the NOAA STAR's monitoring results [12]. WUCD + All C-coefficients are the most stable over time due to the fact that more data are used for their derivation, including large number of granules during the stable nominal operations. However, c_0 values are very sensitive to the subset of data used for fitting. The c_0 coefficients derived using this subset of data represent better scene temperatures closer to the nominal BB temperature, but may not work well for cold scene temperatures. The C-coefficients derived using CD-only data show larger fluctuations over time than those derived using WUCD + All and WUCD + 100 data, indicating

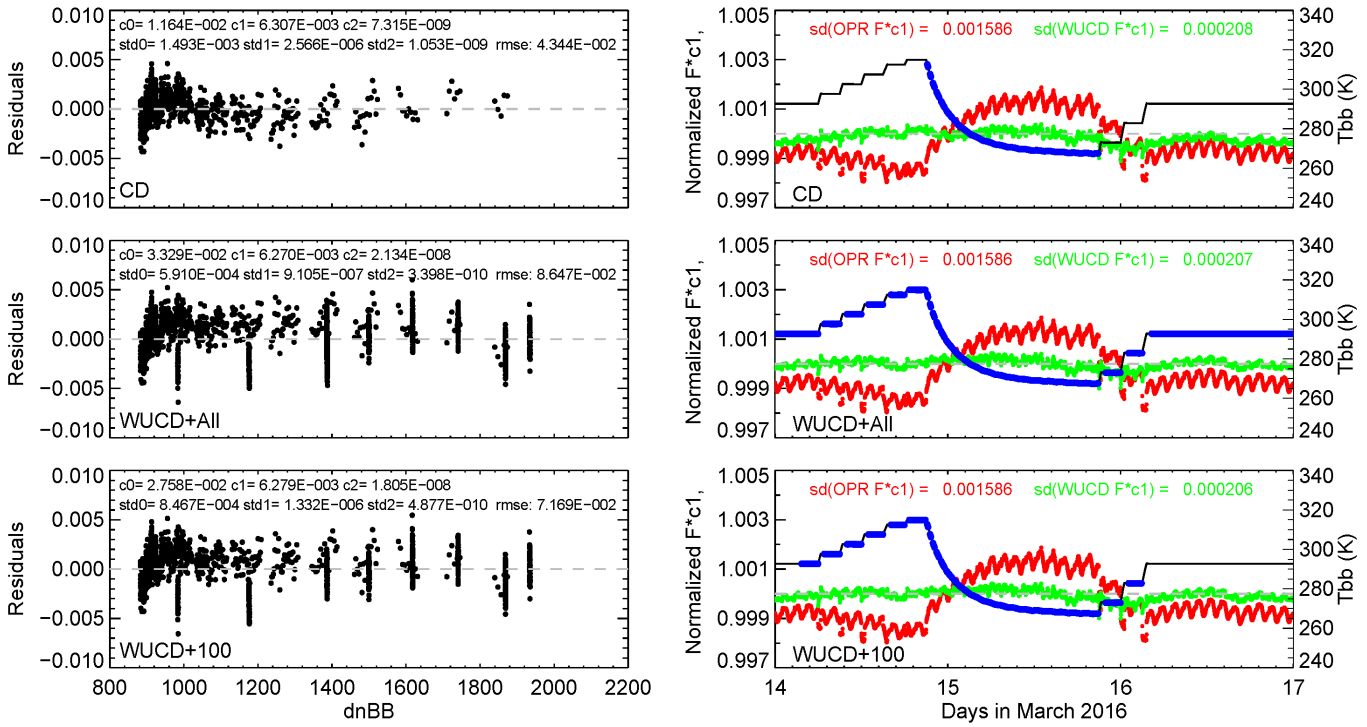

Fig. 11. (Left) Residual errors, in W/(m^2 · sr · μm), of WUCD C-coefficients fitting results using three subsets of data (M15, detector 8, HAM-A); (right) time series of $F \cdot c_1$ for (red curves) prelaunch and (green curves) WUCD-derived C-coefficients. Subset of WUCD data used for fitting is marked by blue color in T_{bb} time series.

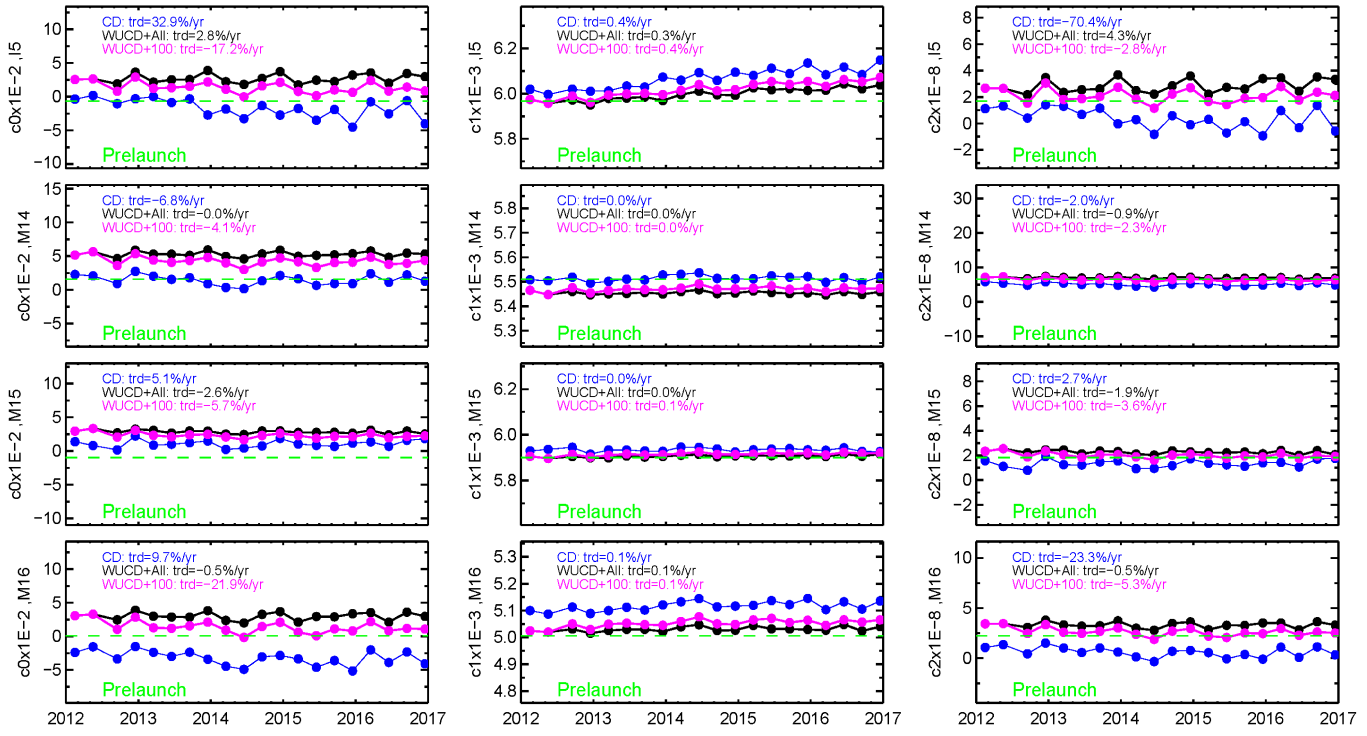

Fig. 12. Band-averaged C-coefficients derived from the three subsets of WUCD data for LWIR bands from Feburary 2012 to December 2016 (I5, M14, M15, and M16). Prelaunch C-coefficients are shown in green for comparison.

that using CD subset may not have sufficient observations at higher radiance levels, to derive stable C-coefficients over time.

Cold calibration bias in band M15 has been reported in [14]–[16]. Our results show that M15 c_0 coefficients derived using the three subsets of WUCD data are persistently higher

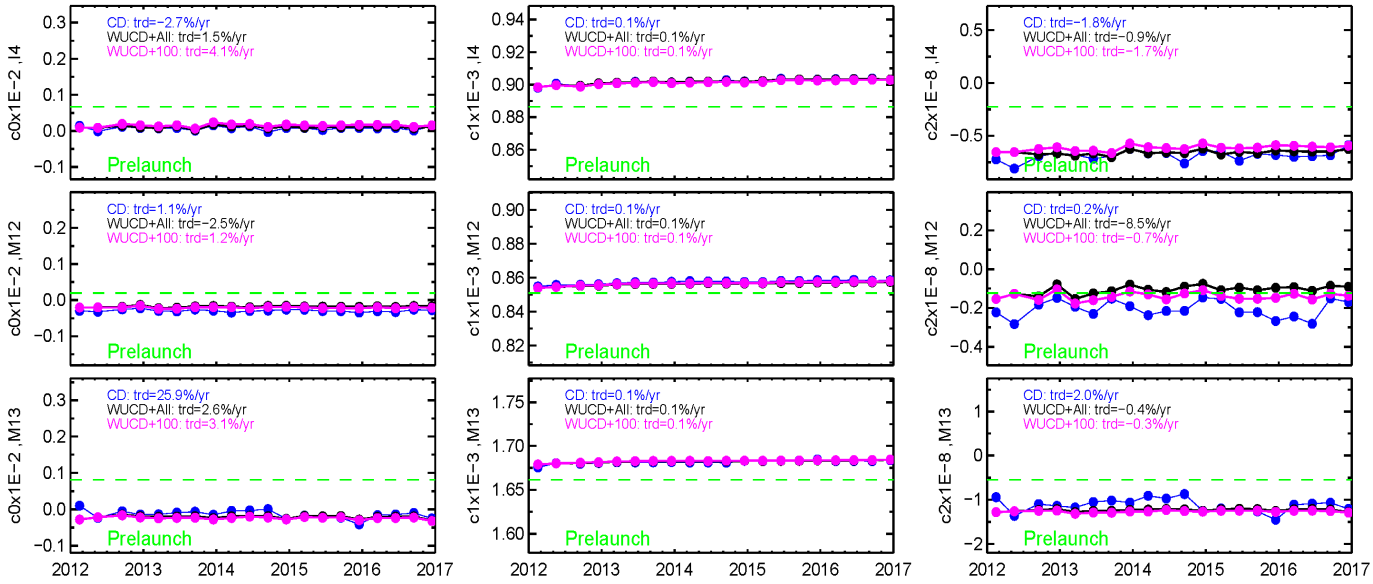

Fig. 13. Band-averaged C-coefficients for the MWIR bands from Feburary 2012 to December 2016 (I4, M12, and M13). Prelaunch C-coefficients are shown in green for comparison purpose.

than the prelaunch values (see Fig. 12), consistent with previous studies. WUCD-derived C-coefficients not only reduce M15 WUCD bias, but may also help reduce the M15 cold bias. More analysis is found in Section IV.

Band-averaged WUCD-derived C-coefficients for the MWIR bands (I4 and M12–M13) are shown in Fig. 13. Compared to the LWIR bands, MWIR band C-coefficients fit using the three subsets of data are generally more consistent with each other, except for c_2. The c_2 coefficients derived using the CD-only data show large fluctuations over time, again indicating that the CD subset does not provide sufficient data samples at all radiance levels, especially at higher radiance levels that are more sensitive to c_2 variations. The performance of the three subsets of C-coefficients for WUCD bias correction will be evaluated in Section IV.

C. Implementation of the WUCD Bias Correction Methods

The Ltrace method introduces a compensatory term to the F-factor calculation [see (6) and (7)]. Code change for the VIIRS TEB calibration algorithm is required to implement this method. Also, new algorithm inputs are required to store WUCD correction parameters. This can be achieved by either introducing a new calibration parameter LUT or modifying an existing one, with the latter requiring significant less code change than the former. In this paper, the VIIRS-SDR-F-PREDICTED-LUT was modified. This LUT is designed to store band, detector, HAM-side, gain, and electronic-side-dependent F-factors, as well as other relevant parameters, for all VIIRS bands, including TEBs. In the OPR, only F-factors for RSBs are used in the RSB offline calibration mode; space reserved for TEB bands are fill values. To implement the Ltrace method, spaces reserved for TEBs were used to control which correction method will be applied and to accommodate Ltrace coefficients. TEB calibration algorithm was also modified to retrieve WUCD method correction coefficients from the LUT, calculate the Ltrace correction term, and apply it to the F-factor calculation. As discussed in Section III, one set of Ltrace coefficients works well during all WUCD events. Therefore, one VIIRS-SDR-F-PREDICT-LUT update is sufficient to implement the Ltrace method.

The implementation of the WUCD-C method requires no code change. Only VIIRS-SDR-DELTA-C-LUT needs to be modified to replace prelaunch values with on-orbit WUCD-derived C-coefficients. The WUCD-derived C-coefficients are also band, detector, and HAM-side dependent. Since no instrument temperature dependence can be derived using on-orbit WUCD data, for each detector, the three 5×5 grid of prelaunch values are replaced by one set of WUCD-derived C-coefficients. Due to the on-orbit degradations of linear response over time, multiple versions of WUCD C-coefficients are required to implement the WUCD-C method. In operational (forward) processing, updated WUCD C-coefficients need to be applied as soon as possible after each WUCD event. In the reprocessing, each version of the C-coefficients should be staged $\sim$1.5 months before a WUCD event.

The selection of optimal WUCD bias correction method and C-coefficients for a band depends on evaludation results and/or F-factor analysis. The two WUCD bias correction methods can be applied on a per band basis. For example, the Ltrace method can be applied to some bands, such as M15 and M16, while the WUCD-C method is applied to the remaining bands, and vice versa. Moreover, C-coefficients derived from different subsets of WUCD data can also be applied on a per band basis.

IV. Evaluation of the Results and Discussion

Reprocessing VIIRS TEB SDRs during all WUCD events require significant amount of computing resources. In this paper, TEB SDRs during two randomly selected WUCD events (September 19, 2016–September 21, 2016 and

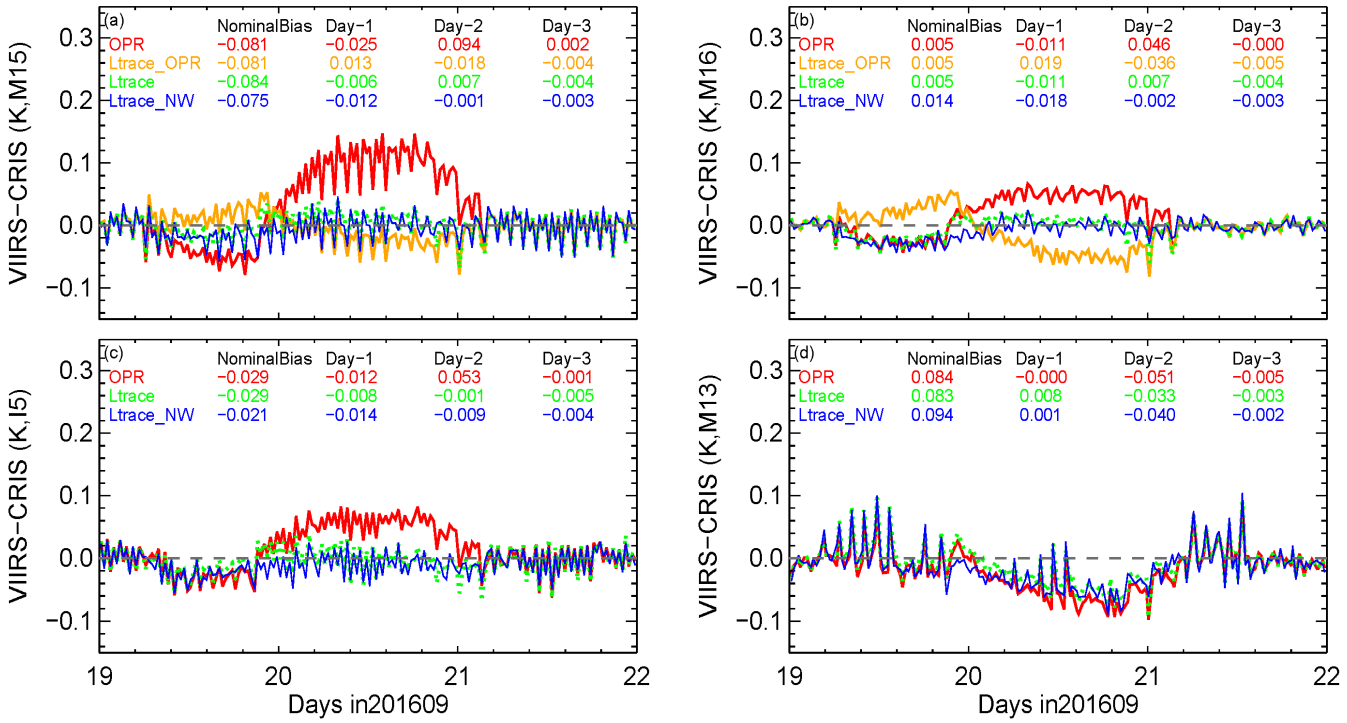

Fig. 14. Time series of VIIRS–CrIS BT difference in (a) M15, (b) M16, (c) I5, and (d) M13 during the September 2016 WUCD event: 1) NOAA OPR (red); 2) same as 1) but after the Ltrace correction (Ltrace_OPR, orange, in M15, M16, only); 3) same as 2), but after the correction of the IDPS C-coefficients implementation error (Ltrace, green); and 4) same as 3), but with nonequal BB thermistor weights (Ltrace_NW, blue).

December 12, 2016–December 14, 2016) were reprocessed to evaluate the two WUCD correction methods, as well as the impact of BB non-uniformity on WUCD biases. The VIIRS SDR algorithm was modified to implement the Ltrace method; the IDPS C-coefficients implementation error was corrected. The Ltrace coefficients were derived from the March 14, 2016–March 16, 2016 WUCD data. As discussed in Section III-A, one set of Ltrace coefficients are good for all WUCD events. For each WUCD event, three sets of WUCD C-coefficien were derived using different subsets of data and applied during the reprocessing accordingly.

A. Validation Using Colocated CrIS Observations

The two WUCD bias correction methods were first evaluated using CrIS observations. CrIS and VIIRS are onboard the same satellite, therefore, providing plenty of colocated independent observations that can be used to evaluate VIIRS radiometric calibration bias during WUCD events. VIIRS bands M15, M16, M13, and I5 are covered by CrIS hyperspectral measurements. Only observations from two nadir CrIS field of regards were used to minimize intercomparison uncertainty, due to errors in geolocation and colocation. A 2-K BT uniformity threshold was used to further reduce intercomparison uncertainty. Moreover, CrIS spectra do not cover the entire spectral range of bands M13, M15, and M16. VIIRS and CrIS out-of-band (OOB) effects were characterized using the Infrared Atmospheric Sounding Interferometer spectra. Band and scene temperature-dependent OOB corrections were applied before computing differences between VIIR and CrIS colocated radiances. Following steps are used to compare VIIRS and CrIS radiance.

1) Colocate CrIS field of views (FOV) with VIIRS pixels using geolocation.
2) Spatially average colocated VIIRS radiances within CrIS FOVs.
3) Spectrally integrate colocated CrIS spectra using VIIRS band-averaged relative spectral response functions to calculate VIIRS equivalent radiances.
4) Correct for VIIRS and CrIS OOB effects.
5) Select spatially homogeneous CrIS FOVs using a 2-K BT threshold, i.e., standard deviations of VIIRS BTs within a CrIS FOV is less than 2 K.
6) Convert averaged VIIRS radiances and integrated CrIS radiances to BTs.
7) Compute VIIRS and CrIS BT differences.

Fig. 14 shows time series VIIRS–CrIS BT differences in bands M15, M16, I5, and M13, under all scene temperatures for the September 2016 WUCD. Similar to Fig. 2, VIIRS–CrIS nominal biases were subtracted from the time series. Statistics of VIIRS–CrIS biases under nominal operations and daily-averaged VIIRS WUCD biases before and after the corresponding corrections are plotted, and their statistics are additionally summarized in Table II.

As discussed in Section III-A, the IDPS C-coefficients implementation error has a significant impact on the Ltrace correction coefficients. Fig. 14(a) and (b) shows that the Ltrace coefficients estimated before the correction of this error over-correct WUCD biases in M15 and M16. The over-correction is small in M15, with daily-averaged residual WUCD bias

TABLE II

STATISTICS OF VIIRS-CRIS BT DIFFERENCES UNDER NOMINAL OPERATIONS AND DAILY-AVERAGED VIIRS WUCD BIASES BEFORE AND AFTER THE CORRECTIONS

		Daily Averaged Biases (K)			
		Nominal	Day-1	Day-2	Day-3
M15	OPR	-0.081	-0.025	0.094	0.002
	Ltrace_OPR	-0.081	0.013	-0.018	-0.004
	Ltrace	-0.084	-0.006	0.007	-0.004
	Ltrace_NW	-0.075	-0.012	-0.001	-0.003
	WUCD-C (WUCD+All_NW)	0.021	-0.008	0.008	0.001
	WUCD-C (WUCD+100_NW)	0.010	-0.005	0.013	0.000
	WUCD-C (CD_NW)	0.000	-0.004	0.019	0.000
M16	OPR	0.005	-0.011	0.046	0.000
	Ltrace_OPR	0.005	0.019	-0.036	-0.005
	Ltrace	0.005	-0.011	0.007	-0.004
	Ltrace_NW	0.014	-0.018	-0.002	-0.003
	WUCD-C (WUCD+All_NW)	0.071	-0.019	0.014	0.003
	WUCD-C (WUCD+100_NW)	0.035	-0.010	0.030	0.002
	WUCD-C (CD_NW)	-0.017	0.002	0.053	0.000
I5	OPR	-0.029	-0.012	0.053	-0.001
	Ltrace	-0.029	-0.008	-0.001	-0.005
	Ltrace_NW	-0.021	-0.014	-0.009	-0.004
	WUCD-C (WUCD+All_NW)	0.052	-0.015	0.005	0.001
	WUCD-C (WUCD+100_NW)	0.023	-0.008	0.018	0.001
	WUCD-C (CD_NW)	-0.011	-0.003	0.038	0.000
M13	OPR	0.084	0.000	-0.051	-0.005
	Ltrace	0.083	0.008	-0.033	-0.003
	Ltrace_NW	0.094	0.001	-0.040	-0.002
	WUCD-C (WUCD+All_NW)	0.080	0.013	0.002	-0.001
	WUCD-C (WUCD+100_NW)	0.080	0.014	0.003	-0.001
	WUCD-C (CD_NW)	0.082	0.009	0.002	-0.002

of −0.018 K on Day 2. However, the over-correction is pronounced in M16, with WUCD biases changed from +0.046 to −0.036 K on Day 2.

After the correction of the IDPS C-coefficients implementation error, the Ltrace method can effectively minimize WUCD biases in the three LWIR bands (M15, M16, and I5), especially on Day 2, to about 0.01 K in all cases. Applying nonequal BB thermistor weights only slightly affects the daily-averaged residual biases (less than 0.01 K). However, it does improve calibration during the WUCD-BB-nonuniform periods, indicated by the suppressed variations in the VIIRS–CrIS BT difference. It also raises scene temperatures by ∼0.01 K under the nominal operations, in all bands. Small under-corrections are observed in all three bands during the warm-up phase on Day 1, which needs to be further investigated in the future. VIIRS–CrIS validation results suggest that the simple linear Ltrace coefficients do not work well for M13, consistent with M13 F-factor analysis results (see Fig. 9). We also evaluated the Ltrace method using the December 2016 WUCD data, and observed similar residual bias patterns.

Fig. 15 shows time series of VIIRS–CrIS BT difference and scene temperature-dependent biases in bands M15, M16, I5, and M13 during the September 2016 WUCD for the NOAA OPR and after the WUCD-C corrections reprocessed with: 1) WUCD + All C-coefficients (WUCD + All_NW); 2) WUCD + 100 C-coefficients (WUCD + 100_NW); and 3) CD-only C-coefficients (CD_NW). Statistics of the corresponding VIIRS–CrIS BT differences are summarized in Table II. Nonequal BB thermistor weights were applied to improve calibration during the WUCD-BB-nonuniform periods. Consistently with the results after the Ltrace correction, it does not significantly affect the daily-averaged WUCD biases. As noted in Section III-B, WUCD C-coefficients, especially c_0, are sensitive to the data used for fitting. When evaluating the performance of the WUCD-C method, it is necessary to monitor scene temperature dependence of the VIIRS–CRIS biases. Moreover, the WUCD-C method is a global method that also affects calibration during nominal operations. Overall, the magnitude of scene temperatures changes are about 0.1, 0.07, 0.08 K, for M15, M16,

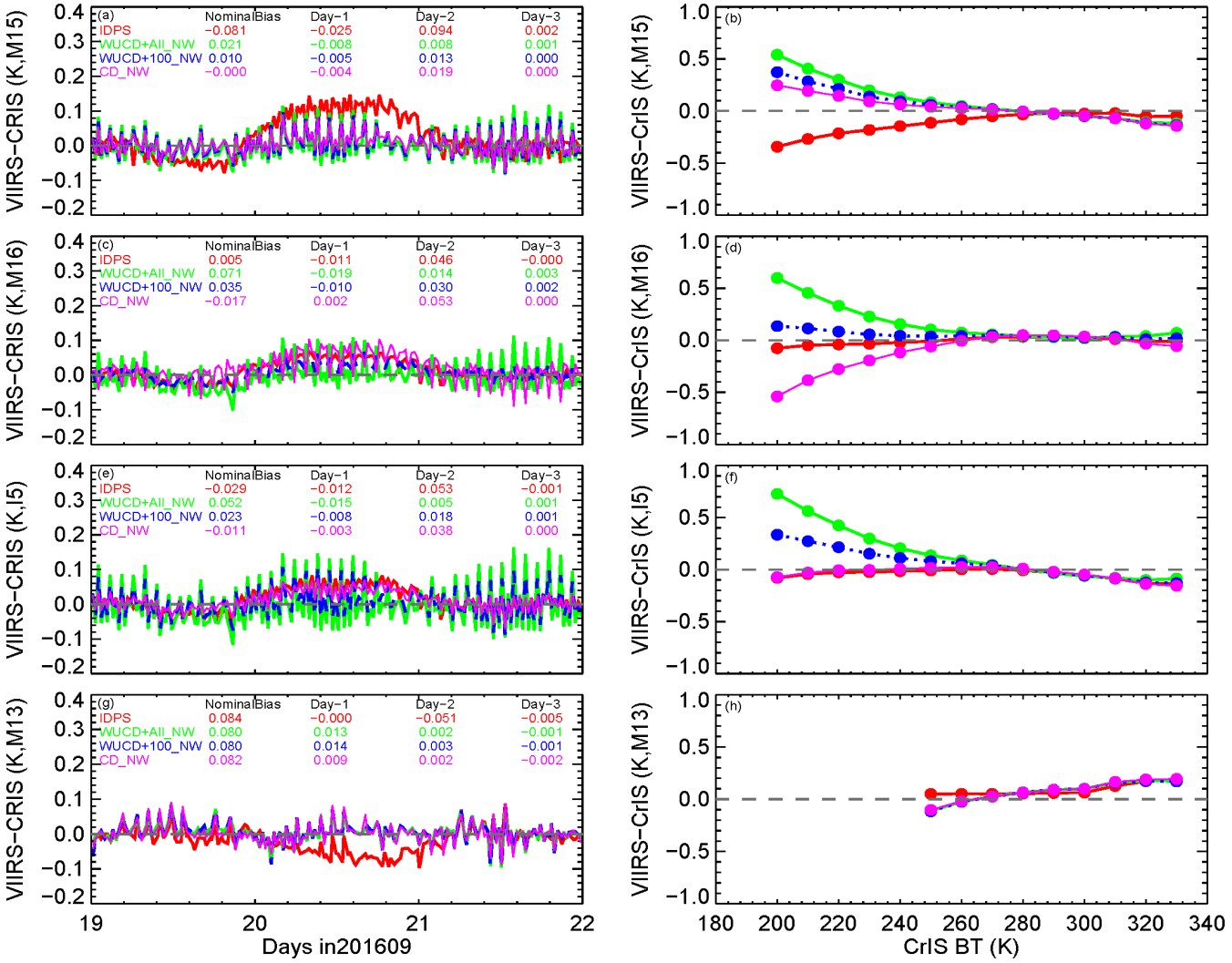

Fig. 15. (a), (c), (e), and (g) Time series of VIIRS–CrIS BT difference and (b), (d), (f), and (h) scene temperature-dependent biases in bands M15, M16, I5, and M13 during the September 2016 WUCD for the NOAA OPR (red) and after the WUCD-C corrections reprocessed with: 1) WUCD + All C-coefficients (WUCD + All_NW, green); 2) WUCD + 100 C-coefficients (WUCD + 100, NW, blue); and 3) CD-only C-coefficients (CD_NW, magenta). Nonequal BB thermistor weights were applied during the reprocessing.

and I5, respectively. Larger corrections occur at cold scene temperatures. The impact on the scene temperatures warmer than 270 K, which are more relevant to SST retrievals, is much smaller, about 0.04, 0.02, 0.03 K, for M15, M16, and I5, respectively. M13 scene temperature does not change much after the WUCD-C corrections.

Fig. 15 (left panel) shows that the WUCD + All C-coefficients perform consistently well in terms of WUCD bias correction in all four bands, with residual WUCD biases on the order of 0.01 K after correction. WUCD + 100 C-coefficients also work for M15, I5, and M13, but underestimate WUCD biases in M16. CD C-coefficients perform reasonably well for M15 and M13, but significantly underestimate WUCD biases in M16 and I5. We also examined the results for scene temperatures representative of SST retrievals. The residual WUCD biases are similar to those under all scene temperatures.

Temperature-dependent biases were also monitored closely to fully evaluate the performances of the three set of C-coefficients. While the WUCD + All C-coefficients work the best among all WUCD-derived C-coefficient to minimize WUCD biases, "warm biases" on the order of 0.5 K at 200-K scene temperatures are introduced for M15, M16, and I5 [see Fig. 15(b), (d), and (f)]. The radiometric calibration uncertainty of CrIS is about 0.2–0.3 K [17], similar to magnitude of "warm biases" introduced by the WUCD-derived C-Coefficients. No conclusion can be made at the current stage. More study is required to fully understand the "warm biases" in the future, as well as their impact on VIIRS environmental data records such as the cloud mask product. Nevertheless, the "warm biases" introduced by the WUCD + All C-coefficients are limited to cold scene temperatures only. Temperature-dependent biases do not change much at warm scenes before and after the WUCD-C correction.

Therefore, this set of C-coefficients can at least be used to reprocess TEB SDRs for SST retrievals.

Time series of VIIRS–CrIS BT difference and temperature-dependent biases in M15 indicate that the C-coefficients fit using CD-only data can be used to minimize both WUCD bias and cold bias in this band. Before the correction, a cold bias on the order of 0.4 K at 200-K scene temperature is observed, in agreement with [15] and [16]. The absolute VIIRS–CrIS bias at 200 K is reduced to about 0.2 K after the correction.

For M13, all three sets of C-coefficients evaluated in this paper work well, with residual bias on the order of 0.01 K [see Fig. 15(g) and (h)]. Moreover, scene temperature-dependent biases do not change significantly after the correction. As shown in Fig. 14, the linear Ltrace correction coefficients do not work well for M13. The WUCD C-coefficients can be used to minimize WUCD bias in this band.

Similar to the results from the Ltrace correction, under-correction during the warm-up phase on Day 1 are also observed in M15, M16, and I5 after the WUCD-C correction. The under-lying cause for the under-correction is still uncertain. After the Ltrace or the WUCD-C corrections, the F-factors during this period are comparable to those during nominal operations (see Figs. 8, 9, and 11), indicating that the residual WUCD biases are not caused by the F-factor anomaly during the WUCD. This remaining issue needs to be studied in the future.

We also analyzed time series of VIIRS–CrIS BT difference and scene temperature-dependent biases using the December 2016 WUCD data, with C-coefficients derived using both September 2016 and December 2016 WUCD events. The December 2016 results agree with results using the September 2016 WUCD data. Moreover, our results indicate that C-coefficients derived from one WUCD event work well for at least three months, until the next WUCD.

B. Validation Using CRTM-Simulated Clear-Sky Radiance

Long-term calibration stability of the NOAA operational VIIRS SDRs has been monitored by the NOAA STAR Monitoring of IR clear-sky radiances over ocean for SST (MICROS; www.star.nesdis.noaa.gov/sod/sst/micros/) [18] and ICVS (www.star.nesdis.noaa.gov/icvs/) [19] systems, using VIIRS-observed BTs minus the Community Radiative Transfer Model (CRTM)simulated BTs (VIIRS-CRTM) in global ocean clear-sky domain. Three TEB M-bands (M12, and M15 and M16) are currently monitored in MICROS and five (M12–M16) in the ICVS [12], [19]. The ICVS data are used here, where VIIRS observations are simulated pixel by pixel using CRTM, with the European Center for Medium range Weather Forecasting reanalysis atmospheric profiles and the Canadian Meteorological Center SST analysis as inputs. Daytime VIIRS-CRTM time series are too noisy to reveal a TEB bias on the order of 0.1 K, due to diurnal cycle effect and solar contamination, but the WUCD biases can be clearly observed in the daily-averaged nighttime VIIRS-CRTM time series [18].

In this paper, we also evaluated the performance of the Ltrace method and the WUCD-C method using global CRTM simulated nighttime clear-sky TOA radiances over ocean. Fig. 16 shows time series of the VIIRS-CRTM BT differences, before and after the corrections (September 10, 2016–October 1, 2016). WUCD + All C-coefficients were used for evaluating the WUCD-C method. Our results show that the noise (3 sigma) in the VIIRS-CRTM time series during nominal operations is about 0.035 K in M12, 0.025 K in M13, 0.040 K in M14, 0.045 K in M15, and 0.060 K in M16. Before correction, daily-averaged WUCD biases on Day 2 (September 20) were about −0.05, −0.06, 0.1, 0.11, 0.09, and 0.02 K for M12–M16, respectively, all beyond the noise levels except for M16. The WUCD biases on Day 1 (September 19) are small and within noise levels. The magnitude of WUCD biases estimated using VIIRS-CRTM and VIIRS–CrIS difference time series are generally consistent. The relatively large differences are only observed in M16 (0.02 versus 0.05 K on Day 2), likely due to differences in the ranges of scene temperatures used by the VIIRS-CRTM (nighttime clear-sky over ocean) and VIIRS–CrIS (daytime and nighttime, over homogeneous colocated observations) match-ups.

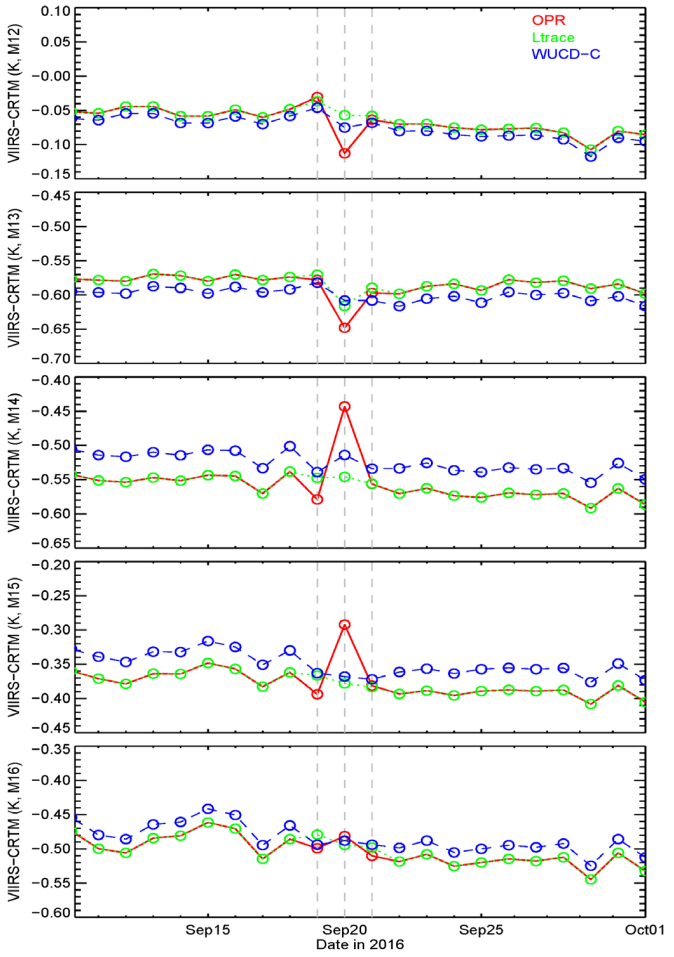

Fig. 16. Nighttime daily-averaged VIIRS-CRTM BT difference time series (M12–M16, September 10, 2016–October 1, 2016) over clear-sky ocean before (OPR, red) and after the Ltrace correction (green) and WUCD-C correction (blue).

The Ltrace method can effectively minimize WUCD biases in M12 and M14–M16 with residual biases bellow noise level (see Fig. 16, green). It also reduces WUCD bias in M13,

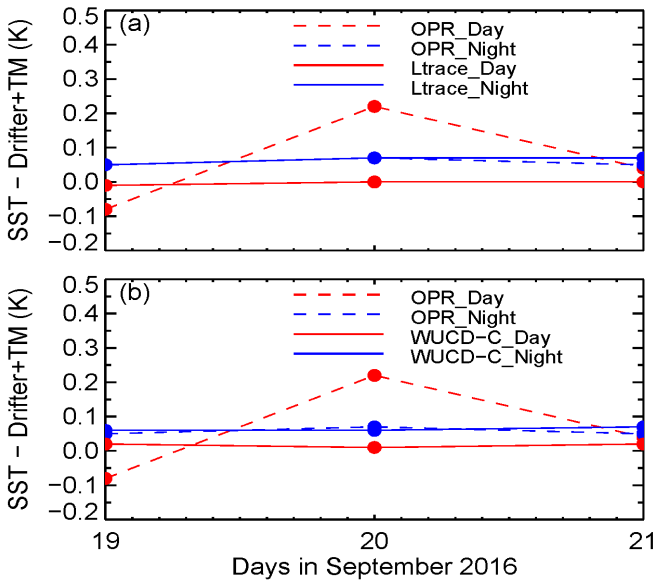

Fig. 17. Global daily-averaged SST anomaly time series during the September 2016 WUCD before and after correction. (a) Ltrace method. (b) WUCD-C method.

however, with a larger residual (0.03 K on Day 2). These results are generally consistent with VIIRS–CrIS validation results for M13, M15, and M16.

The WUCD-C method performs well for all TEB M-bands, with residual biases below noise level in all cases (see Fig. 16, blue). As shown in Fig. 15, for M13 and M15, the performance of the three sets of C-coefficients is very close to each other at scene temperatures for SST retrieval; therefore, validation results shown in Fig. 16 can also be applied for the CD and WUCD + 100 derived C-coefficients. It is worth noting that the WUCD-C method is a global correction method that changes VIIRS BTs over clear-sky ocean by about −0.01 K (M12), −0.018 K (M13), 0.037 K (M14), 0.032 K (M15), and 0.020 K (M16). In Fig. 16, only data during the 3-day WUCD event were reprocessed; VIIRS-CRTM biases during other days were generated using operational products and adjusted by the above estimated differences. The Ltrace and WUCD-C methods were also evaluated using the December 2016 WUCD data, with similar results.

C. Evaluation Using the SST Algorithm

The S-NPP VIIRS TEB WUCD biases that are on the order of 0.1 K have the most pronounced effect on the daytime SST product, among all VIIRS environmental data records [1]. The Ltrace method and the WUCD-C method were further evaluated using the SST algorithm. Fig. 17 compares daily mean differences of the VIIRS minus *in situ* SSTs during the September 2016 WUCD event, before and after the Ltrace and the WUCD-C corrections. The *in situ* data, reported in the NOAA *in situ* Quality Monitor system [20], come from the drifting and tropical moored buoys (hereafter, "Drifter + TM"). Before the correction, daytime SST WUCD anomaly is on the order of 0.25 K on Day 2; no obvious anomaly can be observed on Day 1. Moreover, no significant WUCD anomaly is observed in the nighttime SST time series, due to the fact that the WUCD biases in M12 (−0.05 K) and M15 and M16 (0.05 K) mostly cancel out each other.

Both the Ltrace and WUCD-C methods can effectively minimize daytime SST WUCD anomaly. The impact of small under-corrections in M15 and M16 on Day 1 is unobservable in the daily SST time series. Moreover, both correction methods have little impact on nighttime SST time series (that did not show WUCD anomaly before correction, to begin with). We have also evaluated the two methods using the December 2016 WUCD data, and found that the residual SST WUCD anomalies are comparable to those in September 2016.

V. Conclusion

This paper investigated the S-NPP VIIRS TEB calibration biases during WUCD events and presented two correction methods. Before correction, the daily-averaged WUCD biases are about −0.04 and 0.05 K for I4 and I5, and −0.05, −0.05, 0.11, 0.09, and 0.05 K for M12–M16, estimated by F-factor analysis or using independent validation results. Our results show that TEB WUCD calibration biases are primarily caused by the change in the shape of the calibration curve (F-factor anomaly). The effect of the BB nonuniformity on WUCD biases is small. However, applying nonequal BB thermistor weights can improve calibration during the WUCD-BB-nonuniform periods. The impacts of the IDPS C-coefficients implementation error on TEB SDR products is small; however, the correction of this error is essential to reliably estimate the F-factor anomalies during the WUCD events.

The implementation and evaluation of two WUCD bias correction methods are presented: the Ltrace method and the WUCD-C method. Both correction methods try to flatten F-factors during WUCD events to minimize the WUCD biases. The Ltrace method is a localized empirical-based method that is only applied during WUCD events. One set of Ltrace correction coefficients works well during all WUCDs. The WUCD-C method, on the other hand, is a global method that uses on-orbit WUCD-derived C-coefficients for TEB calibration. The two methods were evaluated extensively using colocated CrIS observations, CRTM simulated nighttime clear sky radiance over ocean, and SST retrieval. Both methods can effectively minimize WUCD-induced SST anomalies. The Ltrace method works well for I5, M12, and M14–M16, with residual biases about 0.01 K. The WUCD-C method, on the other hand, performs well to correct WUCD biases in all TEBs, with residual biases also about 0.01 K. However, it introduces warm biases relative to CrIS at cold scene temperatures in some cases, which requires further study. In addition, the C-coefficients derived from CD data can be used to minimize both the WUCD biases and the cold bias in M15.

In this paper, the performances of the two WUCD bias correction methods for six out of seven VIIRS TEB bands were evaluated using independent measurements. However, band I4 has not been validated due to limitations of the existing validation tools. Under-corrections were observed in the LWIR bands during the warm-up phase. These issues need to be addressed in the future. NOAA-20 was successfully launched on November 18, 2017. NOAA-20 VIIRS SST bands

show smaller WUCD biases than S-NPP, but still introduce visible WUCD anomaly in the daily daytime SST time series. Preliminary results indicate that the two methods presented in this paper also work well for NOAA-20 TEB WUCD bias correction. The methodologies developed in this paper will also be valuable to study and correct TEB WUCD calibration bias in the future J2–J4 VIIRS.

ACKNOWLEDGMENT

The views, opinions, and findings contained in this report are those of the authors and should not be construed as an official NOAA or U.S. Government position, policy, or decision.

REFERENCES

[1] C. Cao, W. Wang, S. Blonski, and B. Zhang, "Radiometric traceability diagnosis and bias correction for the Suomi NPP VIIRS long-wave infrared channels during blackbody unsteady states," *J. Geophys. Res., Atmos.*, vol. 122, no. 10, pp. 5286–5297, 2017.

[2] W. Wang *et al.*, "Operational correction and validation of the VIIRS TEB longwave infrared band calibration bias during blackbody temperature changes," *Proc. SPIE*, vol. 10402, p. 104021P, Sep. 2017.

[3] B. Efremova, J. McIntire, D. Moyer, A. Wu, and X. Xiong, "S-NPP VIIRS thermal emissive bands on-orbit calibration and performance," *J. Geophys. Res., Atmos.*, vol. 119, pp. 10859–10875, Sep. 2014.

[4] A. Ignatov *et al.*, "JPSS SST products at NOAA," presented at EUMETSAT, Toulouse, France, Sep. 2015.

[5] P. Dash, A. Ignatov, Y. Kihai, and J. Sapper, "The SST quality monitor (SQUAM)," *J. Atmos. Ocean. Technol.*, vol. 27, no. 11, pp. 1899–1917, 2010.

[6] C. Cao *et al.*, "Suomi NPP VIIRS sensor data record verification, validation, and long-term performance monitoring," *J. Geophys. Res., Atmos.*, vol. 118, pp. 11664–11678, Oct. 2013.

[7] R. Datla, X. Shao, C. Cao, and X. Wu, "Comparison of the calibration algorithms and SI traceability of MODIS, VIIRS, GOES, and GOES-R ABI sensors," *Remote Sens.*, vol. 8, no. 2, p. 126, 2016.

[8] *Joint Polar Satellite System (JPSS) VIIRS Radiometric Calibration Algorithm Theoretical Basis Document (ATBD)*, document E/RA-00003, VIIRS ATBD, NOAA/NESDIS/STAR, 2013.

[9] J. Xiong, G. Toller, J. Sun, B. Wenny, A. Angal, and W. Barnes, "MODIS level 1B algorithm theoretical basis document," NASA, Washington, DC, USA, Tech. Rep., 2013. [Online]. Available: https://mcst.gsfc.nasa.gov/sites/mcst.gsfc/files/file_attachments/MODIS_L1B_ATBD_ver4.pdf

[10] T. Chang and X. Xiong, "Assessment of MODIS thermal emissive band on-orbit calibration," *IEEE Trans. Geosci. Remote Sens.*, vol. 49, no. 6, pp. 2415–2425, Jun. 2011.

[11] *Joint Polar Satellite System (JPSS) Common Data Format Control Book—External (CDFCB-X) Volumes VIII—Look Up Table Formats*, document 474-00001-08-B0124, JPSS Goddard Space Flight Center, Greenbelt, Maryland, 2015.

[12] ICVS. (Nov. 10, 2017). *STAR Integrated Calibration Validation System*. [Online]. Available: https://www.star.nesdis.noaa.gov/icvs/status_NPP_VIIRS.php

[13] C. Cao, W. Wang, S. Blonski, and B. Zhang, "Preliminary study of the on-orbit radiometric traceability and artifacts for the VIIRS longwave infrared channels during blackbody temperature changes," *Proc. SPIE*, vol. 10403, p. 104030F, Aug. 2017.

[14] W. Wang and C. Cao, "DCC radiometric sensitivity to spatial resolution, cluster size, and LWIR calibration bias based on VIIRS observations," *J. Atmos. Ocean. Technol.*, vol. 32, pp. 48–60, Jan. 2015.

[15] C. Moeller. (May 1, 2013). *S-NPP VIIRS Thermal Emissive Band (TEB) Validation Update*. [Online]. Available: http://www.star.nesdis.noaa.gov/star/documents/meetings/SNPPSDR2013/dayTwo/Moeller_VIIRS.pdf

[16] D. Tobin *et al.*, "Soumi NPP/JPSS Cross-Track Infrared Sounder (CrIS): intercalibration with AIRS, IASI, and VIIRS," presented at the 93rd AMS Annu. Conf., Austin, TX, USA, 2013.

[17] D. Tobin *et al.*, "Suomi-NPP CrIS radiometric calibration uncertainty," *J. Geophys. Res., Atmos.*, vol. 118, pp. 10589–10600, Sep. 2013.

[18] X. Liang and A. Ignatov, "Monitoring of IR clear-sky radiances over oceans for SST (MICROS)," *J. Atmos. Ocean. Technol.*, vol. 28, pp. 1228–1242, Oct. 2011.

[19] X. Liang *et al.*, "Monitoring of VIIRS ocean clear-sky brightness temperatures against CRTM simulation in ICVS for TEB/M bands," *Proc. SPIE*, vol. 10402, p. 104021S, Sep. 2017.

[20] F. Xu and A. Ignatov, "*In situ* SST quality monitor (*i*Quam)," *J. Atmos. Ocean. Technol.*, vol. 31, pp. 164–180, Jan. 2014.

Wenhui Wang received the B.S. and M.S. degrees in computer science from Xi'an Jiaotong University, Xi'an, China, in 1991 and 1994, respectively, and the Ph.D. degree in geography specializing in remote sensing from the University of Maryland, College Park, MD, USA, in 2008.

From 1994 to 2001, she was a Senior Software Engineer with the Institute of Computing Technology, Chinese Academy of Science, Beijing, China. From 2008 to 2013, she was a Support Scientist with I. M. Systems Group, Inc., Rockville, MD, USA. She is currently a Senior Scientist with the Earth Resources Technology, Inc., Laurel, MD, USA, and National Oceanic and Atmospheric Administration/NESDIS/STAR, College Park, MD, USA. Her research interests include satellite instrument calibration and validation, climate data records, surface radiation budget, and geovisualization.

Changyong Cao received the B.S. degree from Peking University, Beijing, China, in 1982, and the Ph.D. degree in geography from Louisiana State University, Baton Rouge, LA, USA, in 1992, with a specialization in remote sensing.

He was a Senior Scientist with five years of aerospace industry experience supporting NASA projects. In 1999, he joined the National Oceanic and Atmospheric Administration (NOAA), College Park, MD, USA, where he is currently a Research Physical Scientist with the NOAA/NESDIS/Center for Satellite Applications and Research. He specializes in the calibration of radiometers onboard NOAA's Operational Environmental Satellites, and currently leads the VIIRS Sensor Science Team, College Park. He has made significant contributions to the international and interagency satellite instrument calibration/validation community, including the Committee on Earth Observation Satellites and World Meteorological Organization Global Space-based Inter-Calibration System.

Dr. Cao was a recipient of two gold and one silver medals honored by the U.S. Department of Commerce for his scientific and professional achievements.

Alexander Ignatov received the M.S. degree in physics from the Moscow Institute of Physics and Technology, Moscow, Russia, in 1982, and the Ph.D. degree (Phys-Math) from MHI, Sevastopol, Russia, in 1989.

From 1982 to 1992, he was a Junior/Research/Senior Scientist with the Marine Hydrophysics Institute, Sevastopol, Russia. He has been with the National Oceanic and Atmospheric Administration Center for Satellite Applications and Research, College Park, MD, USA, since 1992, focusing on remote sensing of ocean, atmosphere, and land. He currently coordinates the development of sea surface temperature retrieval algorithms, including from new generation Joint Polar Satellite System and GOES-R satellites.

Xingming Liang received the Ph.D. degree in remote sensing and atmospheric sciences from Saga University, Saga, Japan.

He was a Research Scientist with the Cooperative Institute for Research in the Atmosphere, Colorado State University, Boulder, CO, USA, and a Visiting Scientist with the National Oceanic and Atmospheric Administration (NOAA)/NESDIS SST Team, College Park, MD, USA, in support for GOESR and JPSS SST Program. He is currently a Support Scientist with the Joint Polar Satellite System VIIRS Calibration Team, Center for Satellite Applications and Research, NOAA/NESDIS. His research interests include development and maintenance of NOAA Integrated Calibration/Validation System, simulation and monitoring of sensor TOA radiances/brightness temperature for Visible Infrared Imaging Radiometer Suite, and application of machine learning in sensor cloud mask for CAL/VAL.

Zhenglong Li received the master's degree in atmospheric sciences from Peking University, Beijing, China, in 2003, and the Ph.D. degree in atmospheric sciences from the University of Wisconsin–Madison (UW), Madison, WI, USA, in 2009.

Since then, he has been a Research Scientist at the Space Science and Engineering Center, UW. He has more than 15 years of experience in meteorological satellite remote sensing, focusing on infrared sounders, both traditional and advanced hyperspectral. His research interests include retrieval algorithm development for atmospheric profiles and land surface emissivity, product validation and evaluation, application to weather forecast and nowcast, and observing system simulation study for future advanced satellites.

Likun Wang received the B.S. degree in atmospheric sciences and the M.S. degree in meteorology from Peking University, Beijing, China, in 1996 and 1999, respectively, and the Ph.D. degree in atmospheric sciences from the University of Alaska Fairbanks, Fairbanks, AL, USA, in 2004.

He was a Post-Doctoral Research Associate with the University of Maryland, College Park, MD, USA, from 2004 to 2005, where he focused on lidar/radar remote sensing of clouds. With more than 12 years of progressive working experiences of National Oceanic and Atmospheric Administration (NOAA)'s satellite sensors (e.g., hyperspectral infrared sounder—Cross-track Infrared Sounder and other infrared sounders—HIRS and SSU) and as research and project management roles, he is responsible for the pre- and postlaunch calibration testing data analysis, intercalibration for postlaunch instrument monitoring and assessment, ground processing software development, configuration and calibration parameter refining, and new algorithm design and integration. He currently serves as a Lead for geometric calibration with the CrIS SDR Team, College Park, MD, USA and the Chair of the World Meteorological Organization sponsored Global Space-based Inter-Calibration System Infrared Sensor Working Group, College Park, MD, USA. He is currently an Associate Research Scientist with ESSIC/CICS, University of Maryland, in support of satellite sensor calibration and validation program for NOAA/NESDIS/STAR, College Park, MD, USA.

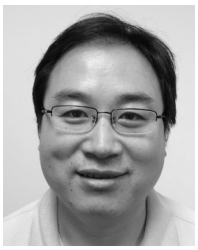

Bin Zhang received the B.S. degree in geophysics from the University of Science and Technology of China, Hefei, China, in 1996, the M.S. degree in physical oceanography from the Institute of Oceanology, Chinese Academy of Science, Qingdao, China, in 1999, and the Ph.D. degree in oceanography from Old Dominion University, Norfolk, VA, USA, in 2008.

He is currently a Satellite Sensor Calibration Scientist with Earth Resources Technology, Inc., College Park, MD, USA, under contract with National Oceanic and Atmospheric Administration /STAR, College Park, MD, USA. He focused Suomi National Polar-orbiting Partnership Visible Infrared Imaging Radiometer Suite calibration/validation/reprocessing, numerical modeling, and data assimilation.

Slawomir Blonski received the master's degree in applied physics from the Gdansk University of Technology, Gdansk, Poland, and the Ph.D. degree in physics from the University of North Texas, Denton, TX, USA.

He currently focuses on calibration and validation of the Visible Infrared Imaging Radiometer Suite instruments and their remote sensing products.

Jun Li received the B.S. degree in mathematics from Peking University, Beijing, China, in 1987, and the M.S. and Ph.D. degrees in atmospheric science from the Institute of Atmospheric Physics, Chinese Academy of Sciences, Beijing, in 1990 and 1996, respectively.

In 1997, he joined the Space Science and Engineering Center, University of Wisconsin–Madison, Madison, WI, USA, where he conducted research on advanced imager/sounder data research and applications, especially on the synergistic use of high-spatial-resolution imager data and high-spectral-resolution infrared sounder data for deriving atmospheric temperature and moisture profiles, cloud and aerosol/dust properties, and surface properties. He is the Principal Investigator of the several GOES-/POES-related projects at SSEC, Madison, WI, USA, including International ATOVS Processing Package (IAPP), GOES-R series trade studies, GOES-R series legacy profile product development, GOES-R series high impact weather studies, Joint Polar Satellite System application for tropical cyclone forecasts, and OSSE for future observations. He has authored or co-authored more than 160 science papers in peer-reviewed journals.

Dr. Li has got several national and international awards during his career for his scientific contributions and achievements, including the 2002 NOAA David Johnson Award and the 2015 University of Wisconsin-Madison Chancellor's Award for Excellence in Research.